Study on boundary conditions in segmental lining design methods

（シールド工法におけるセグメント設計法の境界条件に関する研究）

PHAM THE ANH

Study on boundary conditions in segmental lining design methods

A dissertation submitted

by

PHAM THE ANH

to

Graduate School of Engineering

in partial fulfillment of the requirements

for the degree of

Doctor of Engineering

Academic advisor: Prof. Mitsutaka Sugimoto

Nagaoka University of Technology

Niigata, Japan

February 2020

Acknowledgments

Pham The Anh

February 2020

Table of contents

Chapter 1. Introduction

1.1. General

One of the problems in urban cities nowadays is congestion, and using underground space is a good alternative solution. By going underground, human beings have a new space for many purposes. In other words, the underground space can serve in many forms, but one effective and common way is to use tunnels. For tunnel construction in congested urban areas, attention should be paid to effects on surroundings such as buildings and other life facilities. One efficient method for this is shield tunneling because of its effectiveness in reducing disturbances to surroundings.

A tunnel serves many functions and can be classified into two types, and both are commonly used in urban areas.

- Traffic tunnel: road tunnel, railway tunnel

- Conveyance tunnel: discharge tunnel (i.e., to prevent flooding), freshwater conveyance tunnel, wastewater collector and transport, utility corridor

1.1.1. Shield tunneling method

This is a mechanized tunnel excavation. In this method, a shield machine will dig a horizontal hole through the ground. Although it can be applicable for wide ranges of ground, it is usually done on soft ground. The concept of this method is illustrated in Fig. 1.1. A rotating cutting wheel in front of the machine is used to dig the ground. A set of hydraulic

jacks at the end of machine will push the machine forward against the erected lining. After excavating a certain distance, an erector will pick precast segments to install a new ring.

Compared with the New Austrian tunneling method (NATM) (i.e., the conventional tunneling method, or mountain tunneling), shield tunneling has its advantages and disadvantages.

1) Advantages:

- Less manual labor, utilizes automation

- Safety: no explosives

- Minimizes disturbances to surroundings: adjacent to existing structures

- Does not require much support for ground

- Accommodates underground water

- Faster excavation

- Allows for continuous excavation

- Minimal noise and vibration to environment

2) Disadvantages:

- More costly

- The shape of tunnel is not flexible, based on the shape of machine

- Usually it is applicable for soft ground; hard ground may cause difficulties for the cutting wheel

- Difficult to excavate sharp curves (i.e., curved alignment)

1.1.2. Segmental tunnel lining

In the shield tunneling method, segmental tunnel lining is commonly used. The reason is that this kind of lining can be used as support for excavation and can immediately support the surroundings, especially because most urban cities are on soft ground. Therefore, the segmental lining can be a permanent one-pass system, keeping the tunnel stabilized during and after excavation.

The lining refers to a certain assembly of segments by longitudinal joints and circumferential joints. Fig. 1.2 shows two common types of longitudinal joint arrangement (JSCE, 2016, p.43). In Japan, segment joints and ring joints are commonly used instead of longitudinal joints and circumferential joints. The connection shown in Fig. 1.2a allows for a fast building of rings while the one depicted in Fig. 1.2b intends to make the lining structure more flexible. However, the number of segment types will increase.

When reinforcing the lining structure (for example, by increasing its thickness), the bending moment in the lining will increase, but when it is so thin, it might collapse. Therefore, the flexibility of the lining is considered. This can be achieved by

- reducing the lining thickness, therefore minimizing cost. However, this should consider the capacity of lining under the axial load or thrust from hydraulic jacks (AASHTO, pp. 10–14).

- allocating full or partial hinges at the positions where the bending moment is large

- increasing the number of longitudinal joints

3

As a result, the configuration in Fig. 1.2a is commonly used in cases where internal forces in the lining (i.e., bending moment) are relatively small to maximize its advantages, that is, when the tunnel is built in hard ground. On the other hand, the configuration in Fig. 1.2b is usually employed for tunnels in soft ground, where the ground force on the lining is large.

1.1.3. Factors affecting lining structure design

In the tunnel, the lining is its main structure and is highly important. Its roles are

- to fulfill intended purposes/functions such as maintaining tunnel openings under external loads and durability during its service life,

- to provide necessary functions for tunnel construction such as resisting jack forces, backfill grouting pressure, and other activities during construction.

Therefore, the lining structure should be designed for durability during its service life. The design process is in Fig. 1.3 (JSCE, 2016, p. 52), showing the allowable stress design method (i.e., as differentiated from the limit state design method). It is also noted that both experience and theory are necessary to set the design loads and select the lining structure in the design process.

Because external actions such as ground properties and loads on lining are uncertain, the design work is not a straightforward, deterministic process. In addition, there is no unique design method which can be applied for all tunnels; in the process, different methods can be used (BTS, 2004, p. 98).

Designing a tunnel lining pertains not only to the problem of the lining structure itself but also to the surrounding ground and interaction between ground and lining. Changing the

lining structure does not have much of an effect on ground deformation. When increasing the stiffness of the lining, the ground pressure on the lining rises, and then the stress in the lining also increases. On the other hand, varying ground properties will influence lining behavior significantly. A designer can allow ground displacement to mobilize ground strength by reducing the lining thickness (Kuesel et al., 1996). This way, the ground pressure on the lining will be reduced. In areas with hard ground, it is likely that the dominant force for determining lining structure is construction load. This is because ground load on the lining is relatively small. However, in areas with soft ground, ground load is probably the predominant force instead of construction load. Therefore, the design concept varies depending on ground conditions. Moreover, the aforementioned analysis depicts the interaction between ground and lining.

One of the crucial factors in tunnel lining calculation is ground–lining interaction. In shield tunneling, there exists an annular gap, which is a space between the outer surface of the lining and the surrounding ground (Fig. 1.4). The gap includes the overcutting and tail clearance of the shield machine. Usually, the excavated area is a bit larger than the shield machine, especially when tunneling in a curved alignment, to make the shield machine move easily. This causes a gap between the excavation surface and the shield skin plate. In addition, between the shield machine and the lining at the end of it, layers of wire brushes are installed with grease in between to prevent soil and water from entering the machine. As a result, the total gap will be filled with grouting material to make sure the lining is in full contact with the surrounding ground and the excavation surface is kept stable. Therefore, in reality, many factors affect ground–lining interaction, such as the following:

1) The advance and overcutting of the shield machine in the ground. As a result, the excavation surface is displaced from its original position, and the earth pressure acting on the lining is different from the earth pressure at rest.

2) The grout-filling rate and grout consolidation, that is, whether the gap is filled completely.

3) Grease.

4) Segment erection time.

1.2. Research objectives

The ground–lining interaction at the boundary between the ground and the lining is one of the most crucial factors influencing lining behavior. Although the effects of ground–lining interaction on the normal direction has been investigated intensively, studies on its role in the tangential direction have been few and limited to a specific case (Duddeck and Erdmann, 1985; Kimura et al., 2002). Moreover, there exists a great disparity on using load models and boundary conditions in both research and practice of tunnel lining design. Therefore, this paper aims to clarify the effects of the tangential ground–spring interaction on lining behavior and lining sectional forces through a parameter study using the beam–spring model and ground spring. The parameter study includes the initial tangential earth pressure, tangential ground spring stiffness, normal ground spring stiffness, and overburden load representing deep and shallow tunnels.

Moreover, in this study:

- The term "shallow tunnel" is considered by the relative connection between overburden depth and tunnel diameter, meaning shallow tunneling and shallow tunnel behavior may cause ground surface settlement and affect adjacent structures on the ground surface.

- On the other hand, a deep tunnel is deemed to be located at a depth that causes small effects.

- A tunnel is not just a hole in the ground. It should be converted into a functioning tunnel that accomplishes the intended and required functions. Therefore, apart from structure durability, other functions such as ventilation, lighting, and fire life safety should be considered. These are out of this study's scope.

1.3. Organization of this thesis

This thesis is organized into four chapters.

- Chapter 1 presents a general introduction to the shield tunneling method and segmental tunnel lining. It then presents the factors affecting lining structure design focusing on the interaction between ground and lining. Finally, the objectives of this study are stated.

- Chapter 2 reviews the aspects of tunnel lining analysis and presents the analysis method of the effects of tangential ground–lining interaction on segmental lining behavior using the beam–spring model.

- Chapter 3 presents and discusses the analysis results.

- Chapter 4 provides conclusions and recommendations as well as the limitations of this study and further studies.

Chapter 2. Analysis method

2.1. Introduction

The shield tunneling method is widely used in soft soil especially in urban areas because it is efficient in minimizing disturbances to surroundings. This method commonly uses segmental lining, which consists of segments connected by longitudinal joints and circumferential joints, and its stability is ensured by surrounding ground. There is interaction between the lining and the surrounding ground, constraining the lining in both normal and tangential directions. This mechanism results in reactions from the ground in both directions.

The ground–lining interaction is one of the important factors in tunnel lining calculation. Sometimes, the segmental tunnel linings are coated on their outer surface to protect them from corrosion and water ingress (for example, Fig. 2.1). The epoxy material, which mainly contains plastic, is usually used for the coating. The plastic layer created on the outer surface can reduce the frictional bond between the linings and the ground, which means the ground around the lining can slip relatively. As a result, the load on the linings will change and hence influence tunnel lining behavior. Therefore, it is necessary to understand the role of lining–ground interaction to produce a safe and economical tunnel lining design.

2.2. Literature review

2.2.1. Tunnel lining analysis

Regarding the segmental lining design, this study focuses on the final loading stage due to ground and groundwater since it is a critical stage especially in soft soils and shallow depth

conditions. In the case of the segmental lining design for the final loading stage, the following two methods are commonly used.

The first approach involves analytical solutions (Morgan, 1961; Schulze and Duddeck, 1964; Muir Wood, 1975; Einstein and Schwartz, 1979; Duddeck and Erdmann, 1985; Matsumoto and Nishioka, 1991; Zhang et al., 2017), where the lining is modeled by a continuous beam without longitudinal joints and circumferential joints, and the ground is modeled by springs or a continuum media. In these analytical solutions, initial earth pressure is applied directly on the lining, and then the ground reaction to the lining due to its deformation is assessed. This approach is fast and simple to use. However, it cannot take the complexity of a tunnel into account such as the above-mentioned joints and effects of tunnel construction. In addition, linear elastic behaviors of lining and ground are assumed for the analytical solution.

The second approach is to use numerical analysis. The segmental lining is usually modeled by the beam-spring model as shown in Fig. 2.2, which can consider the effect of staggered arrangement of segments, under the following assumptions: (1) the plane strain conditions in the transverse section for the lining and ground, (2) the linear-elastic behavior of the lining, and (3) the nontension linear-elastic characteristic of the ground. The two rings are connected by circumferential joints, which are modeled by shear springs in the normal and tangential directions. The segments are connected by a longitudinal joint, which is modeled by a rotational spring representing the relation between the rotational angle and moments and is tied at both ends of the segments. On the other hand, the ground is modeled by continuum elements or ground spring in the numerical analysis. The first ground model uses soil continuum elements and ground-lining interface elements to represent surrounding ground and the ground–lining interaction, respectively (Yamada et al., 1986; Fujii et al., 1999; El-Nahhas et al., 1992; Thienert

10

and Pulsfort, 2011; Do et al., 2013; Chaiyaput and Sugimoto, 2016; Vitali et al., 2018). This model can analyze both lining and ground behavior, and offer the ability to model sophisticated properties of ground and lining structure, construction process, and complex scenarios; that is, material nonlinearity, different geological strata, gap-filling process, and effects on adjacent structures. However, it is difficult to simulate their behavior in shallow tunnels in soft ground, needs a lot of computational effort and time-consuming. The second ground model represents the ground–lining interaction by the ground spring and the initial earth pressure in the normal and tangential directions as shown in Fig. 2.3. This model can only analyze lining behavior but is commonly applied in both research and practice on the design of tunnel lining as recommended by most of current tunnel lining design standards (RTRI, 1997; AFTES, 2005; ITA, 2000; BTS, 2004; AASHTO, 2010; DAUB, 2013; JSCE, 2016; BSI, 2016).

In the case of the ground spring model, the initial earth pressure acting on the lining can be modeled by two common load models as shown in Fig. 2.4. Load model type 1 in Fig. 2.4 is composed of the horizontal and vertical earth pressure (Duddeck, 1980; RTRI, 1997; Koyama and Nishimura, 1997; ITA, 2000; Do et al., 2014; JSCE, 2016; Vu et al., 2017), which generate shear stress at the boundary between ground and lining, while load model type 0 in Fig. 2.4 only considers normal earth pressure (Matsumoto and Nishioka, 1991; RTRI, 1997). The normal ground spring in the interaction defines ground reactions in the normal direction against the lining and usually represents only the passive side of earth pressure (e.g. RTRI, 1997; Koyama and Nishimura, 1997; Armau and Mollins, 2011; OVBB, 2011; Do et al., 2014; Vu et al., 2017). The ground reaction curve, which can represent the ground reaction from the active side to the passive side and can include the Winkler spring model, was developed in consideration of the initial displacement of the excavation surface (Sramoon and Sugimoto, 2000). On the other hand,

while the boundary between ground and lining for conventional tunnel is always regarded as full bond, for shield tunnel the tangential ground spring stiffness, k_t, is commonly chosen in a range between 0 and the normal ground spring stiffness, k_n, as shown in Table 2.1. In case of k_t $\cong 0$, which means tangential slip between ground and lining, and the tangential spring is chosen to stabilize the computation (AASHTO, 2010; OVBB, 2011). In tunnel design practice, combinations of the load model types in Figure 2.4 and values of k_t in Table 2.1 are in use. Furthermore, it is noted that load model type 1 contradicts the ground–lining interaction model with small k_t, since the generated tangential stress in case of load model type 1 is not fully transmitted on the lining surface.

Since ground–lining interaction is one of the most crucial factors influencing the results of the analysis, the effect of ground–lining interaction in the normal direction has been investigated intensively, but parameter studies on the role of ground–lining interaction in the tangential direction are few and limited to a specific case only. Duddeck and Erdman (1985) carried out parameter studies on the effect of tangential boundary condition between the ground and lining using analytical solutions without longitudinal and circumferential joints. Kimura et al. (2002) carried out a parameter study on the effect of tangential spring stiffness, normal spring stiffness, the lateral earth pressure ratio and the overburden load using the beam-spring model with ground springs, to simulate the site measured data; that is, a specific case. Moreover, according to the literature review mentioned above, there exists a great disparity on using load models and boundary conditions in both research and practice of tunnel lining design. Therefore, this paper aims to make clear the effects of the tangential ground–spring interaction, of which conditions come from the standards, guidelines, and recommendations on tunnel lining design, on lining behavior and lining sectional forces through a parameter study using the beam-spring

model and ground spring. The parameter study includes the initial tangential earth pressure, tangential ground spring stiffness, normal ground spring stiffness, and overburden load (representing deep and shallow tunnels). The obtained results contribute to our understanding on effects of tangential ground–lining interaction; thus, giving guidelines and information for practitioners regarding the tunnel lining design.

2.2.2. Differences between deep tunnel analysis and shallow tunnel analysis

There are differences between these tunnel lining analyses that pertain to the effects not only on the tunnel lining structure itself but also on the surroundings. The differences are as follows:

- Small soil-covered tunnels are usually located in soft soil.

- Because of small overburden, axial force in the shallow tunnel is small. As a result, the tensile force (caused by bending moment) generated in the segment joints is particularly large.

- The settlement profile of ground surface is different (Fig. 2.5). That is, in the case of a shallow tunnel, roughly all points on the ground surface over the tunnel diameter size have the same settlement. On the other hand, there is a limited area in the case of a deep tunnel.

- A shallow tunnel has generally greater influence on super structures than a deep one.

In the design of a tunnel with small overburden, the problems to consider, which are different from those of the deep one, as shown in Fig. 2.6 (Ishigaki et al., 2016), are the following:

- Tunnel buoyancy: the floating of the tunnel when it is under the groundwater level.

13

- Lining deformation in the vertical axis, that is, as overburden depth increases, (1) the difference between the vertical and horizontal earth pressure at tunnel center becomes larger, and (2) the ratio of the total initial horizontal earth pressure to the total vertical earth pressure becomes larger, as follows:

  · Deep tunnel $= \dfrac{2\sigma_h + 2\sigma_w}{2\sigma_v + 2\sigma_w} = \dfrac{\sigma_h + \sigma_w}{\sigma_v + \sigma_w} = 1 - \dfrac{0.5}{1 + \dfrac{\gamma_w}{\gamma_{soil}}}$, (assume $H \gg D =$ tunnel diameter)

  · Shallow tunnel $= 2\dfrac{\sigma_h + \sigma_w}{\sigma_v + \sigma_w} = 2\left(1 - \dfrac{0.5}{1 + \dfrac{\gamma_w}{\gamma_{soil}}}\right)$,   (assume $H{=}0$)

- Earthquake effects: The impact of earthquakes increases when the tunnel is located in softer soil, nearer to ground surface. Moreover, in case of earthquakes, the relative displacement between the upper and lower parts is large. This causes a large bending moment in the lining.

2.2.3. Determination of earth pressure acting on the lining and ground reaction curves

For tunnels excavated by shield tunneling, the earth pressure acting on the lining depends on many factors:

- Ground characteristics and underground water conditions

- Tunnel shape

- Shield machine operation (influence to surrounding ground and over-excavation)

- Grouting method and grouting rate (grout is needed to fill the gap between lining and tunnel)

- Lining erection time

By using ground reaction curves (Sramoon and Sugimoto, 2000), the earth pressure acting on the lining is simulated continuously from a passive to an active state. The point is that the slope of the curves is defined using the coefficient of subgrade reaction k. This means, when the ground is hard, self-stabilization after a certain displacement of ground can be expected by using these curves. Therefore, the loosening earth pressure is not necessarily mentioned here.

2.2.4. Loosening earth pressure

In tunnel lining design, the determination of load acting on the tunnel is important. When calculating the earth pressure on the tunnel, it is necessary to consider arching action. Arching can occur depending on

- ground conditions: soft or hard

- tunnel type: shallow or deep. In other words, overburden depth is compared to tunnel diameter.

Generally, in the case of soft ground and a shallow tunnel, the arching action of the ground is usually not expected.

The loosening earth pressure may be calculated (JSCE, 2016, p.56) as shown in Fig. 2.7:

$$\sigma_v = \frac{B_1\left(\gamma - c/B_1\right)}{K_o \tan \phi} \cdot \left(1 - e^{-K_0 \tan \bullet H/B_1}\right) + po \bullet e^{-K_0 \tan \bullet H/B_1} \tag{2.1}$$

$$B_1 = R_o \cot\left(\frac{\pi/4 + \phi/2}{2}\right) \tag{2.2}$$

where σ_v: Terzaghi's loosening earth pressure; K_o: ratio of horizontal earth pressure to vertical earth pressure (usually 1.0); ϕ: internal friction angle of soils; p_0: surcharge load; γ: unit weight of soil; and c: cohesion of soil. When p_0/γ is small compared to H, the loosening pressure can be calculated using the following equation:

$$\sigma_v^{'} = \frac{B_1\left(\gamma - c / B_1\right)}{K_o \tan \phi} \cdot \left(1 - e^{-K_0 \tan \bullet H / B_1}\right) \tag{2.3}$$

2.2.5. Segment joint

Lining behavior depends significantly on segment joint stiffness and the number of segment joints in a ring. Segment joint stiffness depends not only on joint type but also on the axial force in the lining. This shows that the interaction between ground and lining affects joint stiffness. According to the experiment shown in the Railway Technical Research Institute (RTRI) standard (RTRI, 1997, p.149-152), k_θ clearly depends on N. The experiment was carried out for several types of bolted joints, and the result is shown in Fig. 2.8 and Tables 2.2 and 2.3.

On the other hand, the rotational spring constant for the modeling segment joint is calculated based on the formula by the Advanced Construction Technology Center (ACTEC, 1999):

$$k_\theta = k_\theta^* \frac{EI_z}{r} \tag{2.4}$$

Accordingly, k_θ is independent from the axial force in the lining. This formula was used to calculate segment joint stiffness for the Neyagawa tunnel project. The segment used in this project is the new mechanical joint (NM) segment. As a result, the joints between segments and between rings do not need bolts (Fig. 2.9).

2.2.6. Interaction between ground and lining

In research and practice, there are common ways to simulate the ground–lining interaction:

- Spring elements: normal and tangential springs. However, it is difficult to determine the relation between tangential and normal interactions.

16

- Interface elements.

- Stress release ratio (for example, it is used in the convergence-confinement method)

The following will review and discuss ways of modeling the interaction.

2.2.7. Touching-spring model

To represent all the effects discussed in section 1.1.3 via Fig. 1.4, the initial displacement of the excavation surface before the lining starts interacting with the ground, u_{init}, from its original position in the normal direction is in use (as shown in Fig. 2.10). The interaction model will consider u_{init} as a displacement boundary condition instead of the stress boundary condition such as the stress release ratio. A positive u_{init} sign shows the outward displacement of the excavation surface.

The interaction is modeled by springs in both normal and tangential directions as shown in Fig. 2.11. The tangential spring is assumed to behave linearly and is independent from the initial displacement, u_{init}. Meanwhile, the normal spring is assigned to simulate the interaction, and its characteristics depend on the initial displacement, u_{init}.

To show a general expression of the initial displacement u_{init}, it is normalized by the tail void and depends on the effective filling rate only as follows:

$$\frac{u_{init}}{t_v} = \alpha - 1 \tag{2.5}$$

where t_v is the tail void, which is calculated from excavation radius by the shield machine and the outer radius of the lining just after excavation, and α is the filling rate of the tail void.

The model can represent all causes by using the initial displacement as follows. The initial displacement, u_{init}, is classified into three cases:

17

a. $u_{\text{init}} = 0$. That is, α is 100% from Eq. (2.5):

This means that before the lining starts interacting with the ground, the excavation surface does not move from its original position; hence, the earth pressure on the excavation surface is equal to the earth pressure at rest at that time (before taking the equilibrium of the whole system). In this case, the normal spring for the lining–ground interaction is assumed to be bilinear as described in Fig. 2.12. Note that u_0 is the required displacement to obtain the earth pressure at rest σ_{n0} on the lining in the bilinear model:

$$u_0 = \frac{\sigma_{n0}}{k_{\text{touching}}} \tag{2.6}$$

where k_{touching} is the constant of the normal spring. In Fig. 2.12,

- $u_n > 0$: the earth pressure on the lining is on the passive side;
- $u_n = 0$: the earth pressure on the lining is at rest;
- $u_0 < u_n < 0$: the earth pressure on the lining is on the active side;
- $u_n \leq u_0$: no earth pressure on the lining.

b. $u_{\text{init}} < 0$, $(\alpha \leq 100\%)$:

This means that before the lining starts interacting with the ground, the excavation surface moves inside the tunnel from its original position. Accordingly, the earth pressure on the excavation surface is on the active side. To obtain the earth pressure at rest, σ_{n0}, on the lining, the required displacement of the excavation surface, u_0, is opposed to its initial movement direction, u_{init}. In this case, at $u_n = 0$, no earth pressure acts on the excavation surface before the lining–ground interaction. Therefore, a bilinear model of the normal spring is proposed and described in Fig. 2.13. In this figure,

- $u_n > u_{\text{init}}$: the earth pressure on the lining is on the passive side;

- $u_n = u_{init}$: the earth pressure on the lining is at rest;
- $u_{init} - u_0 < u_n < u_{init}$: the earth pressure on the lining is on the active side;
- $u_n \leq u_{init} - u_0$: no earth pressure on the lining.

c. $u_{init} > 0$, ($\alpha > 100\%$):

This case means that before the lining starts interacting with the ground, the excavation surface moves outside the tunnel from its original position; hence, the earth pressure on the excavation surface is on the passive side. In this case, there is already passive earth pressure acting on the excavation surface at $u_n = 0$. Therefore, the bilinear normal spring proposed for the interaction works in the way shown in Fig. 2.14.

- $u_n > - u_{init}$: the earth pressure on the lining is on the passive side;
- $u_n = - u_{init}$: the earth pressure on the lining is at rest;
- $- (u_{init} + u_0) < u_n < - u_{init}$: the earth pressure on the lining is on the active side;
- $u_n \leq - (u_{init} + u_0)$: no earth pressure on the lining.

In practice, we do not know which of the three cases will occur. Therefore, the filling rate α is treated as a parameter. In addition, in the normal spring model, a small stiffness is assigned to the "zero-stress" part to avoid numerical errors during calculation. Similarly, the stiffness is not too big to avoid numerical errors (i.e., poor matrix). It is noted that, in this method, the displacement is used for modeling the interaction.

2.2.8. Convergence-confinement method

The convergence-confinement approach (CCM) provides a basic understanding of ground–lining interaction by considering the ground and lining behavior separately (Fig. 2.15). It is used to determine the loading applied to the lining, σ_R, and the normal displacement of the lining, u_R. The ground reaction curve shows the normal active earth stress in soil and is a

function of normal displacement at that point, which is progressively reduced. For the lining, the normal earth stress acting on it is also a function of normal displacement at that point, which is progressively increased. The origin point shows the stress of the ground just before the excavation. The key point in the CCM is to determine the confinement loss, λ_d, that occurs before lining starts interacting with the ground. λ_d is initially set to 0 and is then is increased progressively to 1 to simulate the construction process. Two stress curves are functions of radial displacement, that is, one for the ground (reduction of ground stress on the lining) and one for the lining as shown in Fig. 2.15. The equilibrium is at the intersection of two curves. Here, λ_d is the unloading proportion before lining construction.

This method can predict the deformation of numerous conditions of ground and support (such as NATM tunnel and shield tunnel). However, the limitations of the approach are as follows:

- Considers the active side of ground reaction only

- Does not consider the effect of the bending moment and the effect of joints in the lining

- Restricted to ground in the vicinity of the tunnel

- 2-D modeling only

It is noted that this approach for ground–lining interaction is based on the stress.

2.2.9. Subgrade reaction and elastic modulus of soil

The coefficient of subgrade reaction k is a crucial parameter for tunnel lining design. It is commonly used as a key input data in the beam–spring model to calculate lining behavior and

footing on elastic foundation. If k is not determined accurately, the structure behavior of lining would not be correctly evaluated.

The test for determining k is the plate-loading test. Accordingly, it is calculated as

$$k = P/\delta$$

(2.7)

where P is the load acting on the plate and δ is the displacement of the plate. However, when determining its value at a position where the tunnel is located, this experiment is probably difficult or its value is probably estimated incorrectly because the initial condition of the ground at that depth has changed after excavation.

The coefficient of the subgrade reaction was first proposed by Winkler in 1867 to calculate railway tracks (Hofmann et al., 2019). In tunneling, the subgrade reaction method was applied to calculate the internal forces in the tunnel lining (Schulze and Duddeck, 1964).

Analytical solutions: Muir Wood (1975) devised an equation to obtain k by an analytical solution:

$$k = \frac{3E_s}{(1+v)(5-6v)R}$$

(2.8)

Some authors, such as Zhang et al. (2014), followed Muir Wood's research.

Experimental approach: From the experiment, RTRI (1997) proposed the following:

$$k = 1.58\alpha 3 E_s B_v^{-0.75}$$

(2.9)

where $B_v = 2R$.

Guidelines and standards: Many guidelines on tunnel lining design provide recommendations on the value of k (JSCE, 2016; AASHTO, 2010; DAUB, 2013). The German Tunneling Committee (DAUB, 2013, p. 23) recommended the value of k as follows:

$$k = \frac{E_s}{R} \tag{2.10}$$

The Japan Society of Civil Engineers (JSCE, 2016) provides values of k for each type of ground as shown in Table 2.4. These values are given with the SPT index and descriptions of ground.

Chaiyaput (2016) linked the beam–spring model to the finite element (FE) model by proposing a relationship between the ground subgrade reaction k used in the beam–spring model and Young's modulus E in the FE model. In the FE model, the ground–lining interaction was represented by using spring elements in two directions (Fig. 2.16), that is, the normal direction and the tangential direction. This requires huge effort in constructing a model.

2.3. Methodology

The analysis method used in this research is composed of a beam-spring model as a lining model and a ground spring model with non-linear characteristics as a ground–lining model. The model has been validated by the site data and parameter study (Sugimoto et al., 2019).

2.3.1. Joints in segmental lining model

In the beam-spring model, the spring constants of the circumferential joints in the normal direction, k_{sr}, and the tangential direction, k_{st}, were determined by RTRI (1997):

$$k_{sr} = \frac{192EI_t}{(2b)^3}, \tag{2.11}$$

$$k_{st} = \frac{2L_j hG}{b}, \tag{2.12}$$

$$I_{\mathrm{t}} = \frac{L_{\mathrm{j}} h^3}{12}, \tag{2.13}$$

where E and G are the Young and shear moduli of the segment concrete, respectively; I_{t} is the moment of inertia for the area for one joint; L_{j} is the length between the consecutive joints; and b and h are the segment width and height, respectively.

The spring constant of the longitudinal joints, k_θ, was determined by ACTEC (1999):

$$k_\theta = k_\theta^* \frac{EI_z}{r} \tag{2.14}$$

where k_θ^* is a coefficient based on joint type (1 is used here), I_z is the moment of inertia, and r is the tunnel radius.

2.3.2. Ground–lining interaction

The ground spring for the ground–lining interaction is composed of the normal spring and the tangential one. The deformation characteristics of normal ground springs were determined based on ground reaction curves (GRC), as shown in Fig. 2.17. The shape of GRC, which represents the non-linear characteristics of the ground, has been validated by the two-dimensional elasto-plastic FE analysis (Sugimoto et al., 2019). Furthermore, the GRC has been applied to some similar targets successfully (Sugimoto et al., 2002a,b; 2007; 2010; 2019). The GRC represents the normal ground–lining interaction from the active to the passive side, including ground self-stabilization.

The ground reaction curves in the horizontal and vertical directions are formulated as follows:

$$K_i(u_n) = \begin{cases} (K_{i0} - K_{i\,min}) \tanh\left(\dfrac{a_i u_n}{K_{i0} - K_{i\,min}}\right) + K_{i0} & (u_n \leq 0) \\[4mm] (K_{i0} - K_{i\,max}) \tanh\left(\dfrac{a_i u_n}{K_{i0} - K_{i\,max}}\right) + K_{i0} & (u_n \geq 0) \quad (i=h,v) \end{cases}, \qquad (2.15)$$

where K is the coefficient of earth pressure; subscripts h and v show the horizontal and vertical directions, respectively; and subscripts 0, max, and min indicate K at rest and the upper and lower limits of K, respectively. Here, u_n is the gap from the original excavated surface before excavation to the outer surface of the lining. It is noted that ground self-stabilization and the constant overcut can be represented using the gap instead of the displacement, as shown in Fig. 2.18. a is the gradient of the curves at $u_n = 0$, which can be obtained by

$$a_i = \frac{k_i}{\sigma_{v0}'} \quad (i = h, v) \qquad (2.16)$$

where k is the subground reaction coefficient and σ_{v0}' is the initial effective overburden load at spring line. The coefficient of earth pressure in the normal direction, K_n, can be calculated as

$$K_n(u_n, \theta) = K_v(u_n)\cos^2\theta + K_h(u_n)\sin^2\theta \qquad (2.17)$$

where θ is the angle measured clockwise from the crown to the considered point (Fig. 2.3). The normal earth pressure acting on the lining, σ_n, is

$$\sigma_n = K_n(u_n, \theta)\sigma_{v0}, \qquad (2.18)$$

The tangential ground spring, which transmits the load between ground and lining tangentially, was assumed to be linearly elastic. Thus, the tangential spring force represents shear stresses on the lining.

Fig. 2.19 shows the ground reaction curves for several types of ground. As the k increases, the slope of curves increases. Moreover, it is noted that when ground stiffness, k, increases, the

24

displacement required for the active displacement is significantly reduced. That is, the active pressure on lining reduce to zero fast under $K_{h,v\ min} = 0.0$.

2.3.3. Initial stress state

In case of soft ground, the arching action of ground is not expected. In addition, in case of stiff ground, using the above-mentioned ground reaction curves, the normal earth pressure acting on the lining becomes close to 0 when the ground moves to active side. The above-mentioned GRC can represent both phenomena. Therefore, the loosing earth pressure for the vertical earth pressure is not adopted in this study.

The initial earth pressure along the lining in the normal and tangential directions, σ_{n0} and τ_0, are calculated from the vertical and horizontal effective earth pressure at rest, σ_{v0} and σ_{h0}, as follows:

$$\sigma_{v0} = \gamma H \tag{2.19}$$

$$\sigma_{h0} = K_{h0} \sigma_{v0} \tag{2.20}$$

$$\sigma_{n0} = \sigma_{v0} \cos^2 \theta + \sigma_{h0} \sin^2 \theta \tag{2.21}$$

$$\tau_0 = (\sigma_{v0} - \sigma_{h0}) \sin \theta \cos \theta \tag{2.22}$$

where γ is the soil unit weight, H is the depth of calculation points, K_{h0} is the coefficient of horizontal earth pressure at rest, and θ is the same as in Eq. (2.17). Load model type 0/type 1 in Fig. 2.4 corresponds to the load model on the lining without/with the initial tangential earth pressure, τ_0, respectively. Here, it is noted that the effective earth pressure method can be used as follow: the water pressure is applied to the lining directly, and the effective earth pressure is in use instead of the total earth pressure.

2.3.4. Parameter study

Table 2.5 presents all analysis cases. The tangential spring constant, k_t, was defined by three different methods according to Table 2.1 and was used as a parameter. The initial tangential earth pressure, τ_0, was taken as a parameter, that is, with and without the initial tangential earth pressure, τ_0, as shown in Fig. 2.4. Various ground stiffness from soft ground to stiff ground was considered since it has considerable influence on lining behavior. Here, the coefficients of the subgrade reaction in both vertical and horizontal directions were assumed equal: $k_v = k_h = k$. The overburden depth, h, was selected to represent a shallow tunnel and a deep tunnel because lining behavior changes under different overburden depths.

2.4. Analysis conditions

2.4.1. Site data

Geotechnical data from the Neyagawa tunnel site in Japan (Kojima et al., 2002; Sugimoto et al., 2011) were used for this analysis. The dimensions and material properties of the lining are presented in Table 2.6. The joint spring constants were calculated by Eqs. (2.11) to (2.13). The segmental ring is assembled from eight precast concrete segments connected by longitudinal joints, and the consecutive rings are in a staggered arrangement as shown in Fig. 2.20. The tunnel position and soil properties are shown in Table 2.7 and Fig. 2.21. The Neyagawa tunnel is a deep tunnel where the overburden depth, h, is 37.635 m; the tunnel diameter, D, is 7.87 m; and the overburden ratio, h/D, is 4.78 with a groundwater level of GL-7.126 m. In this study, a shallow tunnel with an overburden depth of 7.87 m, that is, $h/D = 1.00$, was also considered. $K_{hmin} = K_{vmin} = 0.0$ was assumed so that ground self-stabilization is expected

as demonstrated in Figs. 2.17, and 2.19. The K_{hmax} and K_{vmax} values were assumed to be 5.0 based on previous research (Sramoon and Sugimoto, 2000).

Fig. 2.22 shows the distributions of the initial normal and tangential earth pressure at rest and the water pressure around the tunnel ring. This figure shows that the shear components are not small, as they are about 0% to 35% of the normal effective ones for both tunnels.

2.4.2. Analysis model

The lining was divided into 100 beam elements with 100 nodes. To simulate the ground–lining interaction, the two-node springs were used. These springs were connected to the lining at the inner end, and the outer end was fixed outside. In this study, the effective earth pressure method was in use. To represent the ground reaction curves in Fig. 2.17, the initial normal effective earth pressure at $u_n = 0$ is set in the ground spring as a prestress load, and the shape of the ground reaction curve is represented by multilinear relationship between the gap and spring constant of the ground spring (as shown in Eqs. (2.23-2.25)). It is noted that $K_{Hmin} = K_{Vmin} = 0$ in Fig. 2.17 represents the nontension characteristics of the ground, that is, ground self-stabilization. The initial tangential earth pressure was applied to the tangential ground springs as a prestress load, and the water pressure was placed directly on the lining in the normal direction. For the analysis, the finite element solver DIANA (DIANA, 2019) was used. The sign convention is shown in Fig. 2.23 for the bending moment M (+: convex deformation to outside), the axial force N (+: compression force), the gap from the initial excavation surface to the lining in the normal direction u_n (+: toward the outside from the tunnel), and the tangential displacement of the lining u_t (+: displacement to counterclockwise).

$$\sigma_n' = \sigma_{n0}' + \Delta\sigma_n' \tag{2.23}$$

$$\sigma'_{n0} = K_n(0,\theta)\sigma'_{v0} \tag{2.24}$$

$$\Delta\sigma_n = \left(K_n(u_n,\theta) - K_n(0,\theta)\right)\sigma'_{v0} \tag{2.25}$$

Chapter 3. Results and discussions

The influence of each interaction condition on lining behavior was investigated. The results in the even-numbered ring are used because of the bisymmetric results at both rings, which are due to the bisymmetric allocation of longitudinal joints in the analysis model as shown in Fig. 2.20. The lining displacement, the normal effective earth pressure, the tangential earth pressure acting on the lining, the bending moment, and the axial force are shown in Figs. 3.1 and 3.2 for the deep tunnel and shallow tunnel for the ground at $k_n = 10, 100, 1000$ MN/m^3 only because the trends of the results for the ground at $k_n = 50, 500$ MN/m^3 are similar to the others. The results for the ground at $k_n = 50, 500$ MN/m^3 are shown in Appendix A.

3.1. Lining behavior and earth pressure acting on lining

3.1.1. Lining displacement

From the lining displacement in Figs. 3.1a and 3.2a, the following were found:

1. Generally, the shape of deformed ring is flat in the horizontal direction and moves upward. These are due to the following: (1) the initial effective earth pressure in the vertical direction is larger than that in the horizontal direction because $K_{h0} = 0.5$ in this analysis, and (2) the buoyancy is larger than the lining self-weight.

2. As the tangential spring constant, k_t, increases, the deformed ring becomes more circular; that is, the lining deformation becomes smaller. This is because the tangential springs reduce the lining displacement in the tangential direction, and their restraint increases as k_t increases.

3. Compared with load model type 0, that is, the initial shear stress $\tau_0 = 0$, the ring at load model type 1 deforms more in the horizontal direction. This is because τ_0 compresses the ring in the vertical direction and extends it to the horizontal direction at $K_{h0} = 0.5$.

4. As the coefficient of the subgrade reaction, k_n, increases, the deformed ring becomes more circular; that is, the lining deformation becomes smaller. This is because the ground reaction force restricts the lining deformation in the horizontal outward direction and increases with larger k_n.

5. Compared with the shallow tunnel, the lining at the deep tunnel deforms more in the horizontal direction, and the diameter of the lining decreases. This is because as the overburden depth increases, (1) the larger difference between the initial vertical effective earth pressure and the initial horizontal effective earth pressure requires more lining deformation to redistribute the effective earth pressure, and (2) under the increase in water pressure, the lining shrinks more that is, axial shortening induced by the compressive axial force in lining.

3.1.2. Normal effective earth pressure

The normal effective earth pressure, σ_n', can be obtained by substituting the gap from the original excavated surface before excavation to the outer surface of the lining, u_n, to Eq. (2.18). Therefore, the σ_n' tendency can be explained by u_n. Usually, u_n is equal to the displacement of the excavated surface in the normal direction except the existing gap between the excavated surface after excavation and the outer surface of the lining because of ground self-stabilization as shown in Fig. 2.18. In this study, the self-stabilization of the ground occurs only at $k_n = 1000$ MN/m^3 and at the deep tunnel.

From the normal effective earth pressure along the lining, σ_n', in Figs. 3.1b and 3.2b, the following were found:

1. The distribution shape of σ_n' is more circular than that of the initial normal effective earth pressure, σ_{n0}'. This comes from the redistribution of σ_n' due to the lining stiffness. Furthermore, σ_n' is close to 0 around the invert at $k_n = 1000$ MN/m³ and the deep tunnel. This is because (1) under the high water pressure, the segmental ring shrinks (i.e. axial shortening induced by compressive axial force), (2) the large k_n reduces the normal displacement of the excavated surface for ground self-stabilization, and (3) the buoyancy, which is larger than the self-weight of the lining, lifts the lining.

2. As k_t decreases and the load model changes from type 0 to type 1, the distribution shape of σ_n' becomes more flat in the horizontal direction. These trends reflect the lining displacement.

3. As k_n increases, σ_n' decreases and the distribution shape of σ_n' becomes more flat in the horizontal direction. These are because (1) the high water pressure in the deep tunnel reduces the lining diameter, (2) a larger k_n decreases σ_n' under the same displacement in the active side, and (3) as k_n increases, the σ_n' around the invert and crown decreases more than the σ_n' at the spring line under the displacement in the active side because $K_{h0} = 0.5$.

4. For $k_n \leq 100$ MN/m³, the σ_n' at the deep tunnel is larger than that at the shallow tunnel, and for $k_n = 1000$ MN/m³, the tendency of σ_n' is in reverse. This is because (1) the deeper tunnel

has the larger initial normal effective earth pressure, σ'_{n0}, and the larger water pressure, σ_w, and

(2) a higher σ_w reduces the lining diameter and σ'_n more, especially for $k_n = 1000$ MN/m^3.

3.1.3. Tangential earth pressure

From the tangential earth pressure, τ, around the lining in Figs. 3.1c and 3.2c, the following were found:

1. The shape of the τ distribution is an ellipse whose major axis has an angle of 45 degrees against the vertical axis, as the loads acting on the lining and the lining structure are almost biaxially symmetric against the horizontal and vertical direction.

2. As k_t increases, (1) for load model type 1 (with τ_0), the distribution shape of τ becomes more circular than that of the initial tangential earth pressure, τ_0, which corresponds to τ under $k_t / k_n = 0$; and (2) for load model type 0 (no τ_0), the distribution shape of τ becomes more flat than that of $\tau = 0$, which corresponds to τ at $k_t / k_n = 0$; and (3) the load model type, that is, the initial tangential earth pressure, τ_0, has more effect on the tangential earth pressure, τ. These are due to the following: (1) The shear stress magnitude is proportional to relative displacement and k_t. Shear stress is generated in the opposite direction of the relative displacement of the lining against the ground. As the analysis condition in this study, the relative displacement direction is horizontally outward as shown in Figs. 3.1a and 3.2a. (2) The direction of the initial tangential earth pressure, τ_0, for load type 1 in Fig. 2.22 under $K_0 < 1$ is also in the horizontal outward direction. (3) The calculated τ comes from the superposition of the above shear stresses.

3. As k_n increases, (1) for $k_t / k_n = 0$, the shape of the τ distribution is almost the same, and (2) for $k_t / k_n > 0$, that becomes more circular. These are because, as k_n increases, (1) the lining

deformation decreases because of the increase in ground reaction force; (2) k_t increases for k_t / k_n > 0; and finally, (3) the relative displacement between lining and ground decreases as shown in Figs. 3.1a and 3.2a.

4. The τ at the deep tunnel is larger than that at the shallow tunnel. This is because the overburden load increases, (1) the relative displacement between lining and ground is larger as shown in Figs. 3.1a and 3.2a; and (2) for load model type 1, the initial tangential earth pressure, τ_0, is larger.

3.2. Cross-sectional forces

3.2.1. Bending moment

Figs. 3.1d and 3.2d show the distribution of bending moment M for the deep tunnel and the shallow tunnel, and Fig. 3.3 shows the maximum and minimum moment (M_{max}, M_{min}), respectively. From these figures, the following were found:

1. The distribution shape of M is flat in the horizontal direction.

2. The distribution shape of M becomes more uniform as k_t and k_n increase, load model type 0 is compared with load model type 1, and the overburden decreases.

3. For $k_n \leq 100$ MN/m^3, the maximum value of the absolute M shows a maximum of a 23% reduction as k_t/k_n increases from 0 to 1, and they show approximately a 58% increment as the load model changes from type 0 to type 1. For $k_n \geq 500$ MN/m^3, the magnitude of M becomes close to zero. These can be explained as the same as in section 3.1.1 (Lining displacement) since the distribution of M basically reflects the lining deformation in Figs. 3.1a and 3.2a.

4. The M at the longitudinal joints of the ring is close to 0; on the other hand, around these longitudinal joints, the M in the next ring has a maximum/minimum value, especially $k_n \leq 100$ MN/m^3. These are because (1) the bending stiffness of the longitudinal joints is smaller than that of the segment itself, and (2) a certain moment in one ring is transferred through the next ring by the circumferential joints in the case of staggered arrangement.

5. In the case of the deep tunnel, a very stiff ground ($k_n = 1000$ MN/m^3), $k_t/k_n = 0$, and the load model is type 1, M fluctuates significantly at the lower part while in other cases, the M distributions are more stable. This is because (1) when $k_t/k_n = 0$ and the load model is type 1 (with τ_0), the lining deforms most flat in the horizontal direction; (2) when k_n is larger, ground self-stabilization is expected with a small active displacement; (3) in the deep tunnel, high water pressure makes the lining shrink, that is, the displacement in the active side appears; (4) because of buoyancy, the tunnel moves upward; (5) the segments are installed in staggered arrangements; and (6) therefore, while the upper part of the lining is supported by the ground, the lower part of the lining can move freely in the normal direction because of the gap between lining and ground as shown in Fig. 3.4, which presents the lining displacements in the normal and tangential directions, u_n and u_t, in the case of $k_n = 1000$ MN/m^3 at the deep tunnel. Thus, M has peaks at the longitudinal joints of the next rings at the lower part.

3.2.2. Axial force

The axial force in the segmental lining, N, results from the normal force on the lining, such as normal effective earth pressure and water pressure; the tangential force on the lining, such as the tangential force due to the tangential springs and the tangential earth pressure due to the load model; and the vertical force due to the self-weight of the lining. Therefore, the axial

force distribution is determined by the normal effective earth pressure in section 3.1.2, the tangential earth pressure in section 3.1.3, the water pressure, and the self-weight of the lining.

Figs. 3.1e and 3.2e show the distribution of axial force for the deep tunnel and the shallow tunnel, respectively. Fig. 3.5 shows the maximum axial force N_{max}, and Fig. 3.6 shows the F_h/F_v ratio defined as follows:

$$\frac{F_h}{F_v} = \frac{N_C + N_I}{N_L + N_R},$$ (3.1)

where N_L, N_R, N_C, and N_I are axial forces in the lining at the left and right spring line, crown, and invert, respectively. F_h/F_v shows the shape of axial force distribution, which becomes horizontally long for $F_h/F_v < 1$ and vertically long for $F_h/F_v > 1$ (Fig. 3.7).

From these figures, the following were found:

1. The distribution shape of N is flat in the horizontal direction while that of σ_n' is flat in the vertical direction. This is because the N comes from the σ_n', initial tangential stress τ_0, tangential stress τ due to k_t, water pressure σ_w, and the self-weight of the lining.

2. As the tangential spring stiffness, k_t, increases, F_h/F_v increases, that is, the distribution shape of N deforms to the vertical outward direction and the horizontal inward direction. This is because the tangential spring restricts the lining deformation to be flat in the horizontal direction under $K_{h0} = 0.5$, and it causes the compression force to the lining in the horizontal direction and the tensile force to the lining in the vertical direction.

3. As the load model changes from type 0 to type 1, F_h/F_v decreases, that is, the distribution shape of N changes from being flat in the vertical direction to being flat in the horizontal direction. This is because the shear earth pressure generates the shear force on the lining to the

35

horizontal outward direction, and it causes an increase in N in the vertical direction and a decrease in N in the horizontal direction. This tendency is reverse to that caused by k_t.

4. The coefficient of subgrade reaction k_n and the overburden depth influence the magnitude of N_{max} in Fig. 3.5 but do not affect the distribution shape of N as shown in Figs. 3.1 and 3.2. These can be explained the same way as σ_n' in section 3.1.2 (Normal effective earth pressure).

5. As for N_{max} in Fig. 3.5, as k_t increases, N_{max} increases for load model type 0, and N_{max} decreases for load model type 1. This is because N_{max} appears at the invert for load model type 0 and at the spring line for load model 1, as shown in Figs. 3.1, 3.2 and 3.6, and the influences of k_t on F_H and F_V are reverse.

6. As k_n increases and overburden depth decreases, N_{max} in Fig. 3.5 decreases. These can be explained the same way as σ_n' in section 3.1.2 (Normal effective earth pressure).

7. While the N distribution becomes smoother as k_n increases, the N distribution bends at the segment joints of the next rings in the case of $k_n = 10$ MN/m^3. This can be explained as follows: with lower k_n , (1) the deformation of the lining is larger, (2) the bending angle at the segment joint increases since the bending stiffness at the segment joints is smaller than that of the segment section, and (3) a larger compression strain is generated at the segment joints of the next ring, that is, a larger N appears.

8. In the case of $k_n = 1000$ MN/m^3, $k_t/k_n = 0$ and load model type 1, the N around the spring line is larger than the N at other positions (F_h/F_v is smallest). This is because (1) no constraint occurs in the tangential direction due to $k_t/k_n = 0$, (2) σ_n' is close to 0 as explained in section

36

3.1.2 (Normal effective earth pressure), and (3) the initial earth pressure τ_0 due to load model type 1 and the self-weight of the lining generate the N directly.

3.2.3. Normalized eccentricity

Bending moment causes the bending stress (i.e. tensile stress) in the segment. On the other hand, the axial force in lining, which is compressive force, causes compressive stress. Therefore, to examine the effect of the parameters on the lining behavior, the combination of M and N should be examined. The eccentricity e normalized by the segment thickness t is used. The eccentricity e is defined as

$$e = \frac{M_{max}}{N_{assoc}} \tag{3.2}$$

where M_{max} is the maximum moment and N_{assoc} is the associated axial force at M_{max}. When e/t is larger than 1/6 ($\cong 0.167$), the tensile stress appears in the segment (Fig. 3.8).

Fig. 3.9 shows the e/t for the deep tunnel and the shallow tunnel, respectively. From Fig. 3.9, the following were found:

1. e/t is larger than 0.167 at $k_n = 10$ MN/m³ for the deep tunnel and at $k_n < 50$ MN/m³ for the shallow tunnel while e/t is negligibly small at $k_n \geq 500$ MN/m³. These are the results of the M distribution and N distribution in Figs. 3.1 and 3.2. This indicates that earth pressure should be considered carefully in soft soils at a shallow tunnel since a tensile stress appears in the lining.

2. As the tangential spring constant, k_t/k_n, increases from 0 to 1, e/t decreases, but the change is less than 0.05. This indicates that the influence rate of k_t on M_{max} and N_{assoc} is similar, and the effect of k_t on e/t is limited.

3. As the load model changes from type 0 to type 1 under $e/t > 0.167$, e/t increases about 1.4 times for the deep tunnel and about 1.7 times for the shallow tunnel. This indicates that the load model type (i.e. τ_0) influences e/t significantly.

4. With larger k_n, e/t is drastically reduced. This means that absolute M_{max} decreases more than N_{assoc} as k_n increases.

5. The e/t at the shallow tunnel is at most about 1.6 times the e/t at the deep tunnel. This means that absolute M_{max} decreases less than N_{assoc} as the overburden depth h decreases since the difference of the initial effective earth pressures at the crown and invert is constant, but the initial vertical effective earth pressure decreases as h decreases.

3.2.4. Earth pressure supported by the lining

Fig. 3.10 shows the support ratio of the initial effective earth pressure by the lining in the vertical and horizontal directions, r_v and r_h, defined as

$$F_{i0} = \sigma'_{i0} \times D \quad (i = h, v) \tag{3.3}$$

$$\begin{cases} F_{ev} = N_L + N_R - \sigma_w \times D - W/2 \\ F_{eh} = N_C + N_I - \sigma_w \times D \end{cases} \tag{3.4}$$

$$r_i = \frac{F_{ei}}{F_{i0}} \quad (i = h, v) \tag{3.5}$$

where F_0 is the initial force on the tunnel section due to the initial effective earth pressure σ'_0; F_e is the force due to the effective earth pressure supported by the lining; N_L, N_R, N_C, and N_I are axial forces in the lining at the left and right spring lines, crown, and invert, respectively; σ_w is the water pressure at the tunnel center; D is the tunnel diameter; W is the self-weight of the lining; and the suffixes v and h show the vertical and horizontal directions, respectively (Fig. 3.11). Here, in the case where the support ratio of the initial effective earth pressure σ'_{i0} by the

38

lining, r_i (i = h and v), is less than 1, the rest of σ'_{i0} is expected to be supported by the surrounding ground. On the other hand, in the case where r_i (i = h and v) is larger than 1, the ground reaction force acting on the lining is larger than σ'_{i0}. For the deep tunnel, F_{v0} = 2864 kN/m and F_{h0} =1432 kN/m, and for the shallow tunnel, F_{v0} = 1176 kN/m and F_{h0} = 588 kN/m.

From Fig. 3.11, the following were found:

1. $r_v < 1 < r_h$ is for $k_n \leq 100$ MN/m^3 while r_v is close to 0, and $r_h < 1$ for k_n = 1000 MN/m^3. This is because (1) for $k_n \leq 100$ MN/m^3, the effective earth pressure acting on the lining, σ'_n, at the crown and invert are at the active side, and the σ'_n at the spring line is at the passive side due to ground reaction, and (2) for k_n = 1000 MN/m^3, σ'_n is always at the active side and σ'_n is close to zero at the deep tunnel due to ground self-stabilization, as shown in Figs. 3.1b and 3.2b.

2. As the tangential spring constant, k_t, decreases and the load model type changes from type 0 to type 1, r_v increases and r_h decreases. This tendency can be explained as the same as in section 3.1.3 (Tangential earth pressure).

3. As the coefficient of the subgrade reaction, k_n, increases, r_v and r_h decrease. This is because as k_n increases, σ'_n drops more in the active side as described in section 3.1.2 (Normal effective earth pressure). Furthermore, r_v and r_h have almost the same value at the deep tunnel and shallow tunnel. This means that the influence rate of the overburden depth on the initial effective earth pressure σ'_0 and the effective earth pressure σ'_n is almost the same in this analysis condition.

3.3. Summary

A parameter study was conducted to investigate the effects of ground–lining interaction in the tangential direction on lining response using the beam-spring model and ground springs. Tangential ground spring stiffness k_t, load model type (the initial tangential earth pressure, τ_0), normal ground spring stiffness k_n, and overburden depth h were used as parameters. As a result, the following were found:

1. The distribution of normal effective earth pressure acting on lining σ_n' mainly obtains the influence of k_n and h, and the distribution of tangential earth pressure acting on lining τ is influenced by k_t and the load model type (i.e. τ_0). Lining displacement is defined by σ_n', τ, and buoyancy and determines the distributions of bending moment, M. The distribution of N is determined by σ_n', τ, water pressure σ_w, and the lining self-weight. The influence of each parameter is propagated through the above mechanism.

2. The k_t restricts the lining displacement in the tangential direction, and the axial force in the lining is generated in the opposite direction of the lining displacement. Therefore, as k_t/k_n changes from 0 to 1: (1) The deformed ring and distribution shapes of M and N become more circular. (2) For $k_n \leq 100\text{MN/m}^3$, the absolute M decreases at most to 23%. For $k_n \geq 500 \text{ MN/m}^3$, the magnitude of M becomes close to zero. (3) The N_{max} changes within 5%. And (4) the change of the normalized eccentricity, e/t, is less than 0.05.

3. The shear stress appears at the boundary toward the spring line for load model type 1 under $K_{h0} < 1$. Therefore, as the load model changes from type 0 to type 1, (1) the deformed ring and distribution shapes of M and N become flat in the horizontal direction; (2) for $k_n \leq 100 \text{ MN/m}^3$, the absolute M increases to at most 58%; (3) the N_{max} increases at most to 9%; and (4)

under $e/t > 0.167$, e/t increases 1.4 times for the deep tunnel and 1.7 times for the shallow tunnel. The case of $e/t > 0.167$, which means tensile stress appears in the lining, corresponds to $k_n = 10$ MN/m^3 for the deep tunnel and $k_n < 50$ MN/m^3 for the shallow tunnel. These indicate that the load model has significant effects on sectional forces, especially at shallow tunnels in soft soils.

4. As k_n increases, under the same displacement, the normal effective earth pressure σ'_n increases at the passive side and decreases at the active side. As a result, the deformed ring and distribution shapes of M and N become more circular, and M, N, and e/t are drastically reduced at $k_n \geq 500$ MN/m^3.

5. As the overburden depth, h, decreases, the effective earth pressure σ'_n and water pressure σ_w decrease, but the difference of the initial effective earth pressures at the crown and invert is constant. Then, (1) the deformed ring and the distribution shape of M become more circular, (2) N decreases, and (3) e/t decreases about 1.6 times.

6. In the case of a shallow tunnel in soft soil where $e/t > 0.167$, tensile stress appears in the lining. Therefore, the tangential ground–lining interaction conditions, such as the initial tangential earth pressure due to load model and the tangential spring constant should be taken carefully since these conditions significantly influence the bending moment in the segmental lining.

7. In the case where the support rates of initial effective earth pressure by the lining in the vertical and horizontal direction, r_v and r_h, are less than 1, which means that the effective earth pressure at the active side around the tunnel appears, the existence of an arching effect, that is, the support of partial initial effective earth pressure by surrounding ground, should be confirmed especially in the case of a shallow tunnel in soft ground.

41

Chapter 4. Conclusions and recommendations

A parameter study has been conducted on the effects of tangential interactions on tunnel lining behavior, that is, load models, boundary conditions between tunnel lining and surrounding ground, ground stiffness, and overburden depth, which represent deep and shallow tunnels. The beam–spring model for representing the tunnel lining structure and the ground springs for the surrounding ground are used to evaluate lining behavior. The parameter study was carried out based on conditions from existing literature. The results contribute to our understanding of the effects of tangential ground–lining interaction, thus, providing guidelines and information for practitioners regarding tunnel lining design.

The findings of this study are summarized as follows:

(1) Tangential spring has small effects on lining behavior, that is, on the bending moment in the segment.

(2) The load model significantly affects the sectional forces, which increase the bending moment in the lining, especially in soft soils and shallow tunnels.

(3) The initial tangential earth pressure and the slip ground–lining boundary provide more safety from a design viewpoint.

(4) In the case of shallow tunnels in soft ground, tensile stress appears in the lining, which can cause an increase in steel bars for reinforcement or a change in lining structure.

Therefore, it is important to consider the tangential ground–lining interaction conditions and the existence of the arching effect, as these conditions significantly affect the bending moment in the segmental lining.

However, the limitation of this work is that when a gap occurs between the ground and the lining, the tangential spring still works in this analysis model. This is the drawback of using spring elements for modeling the ground–lining interaction. The interface elements with the finite element model can be employed to eliminate this disadvantage.

For further studies, it is recommended that the gap between the lining and the original excavation surface before excavation should be considered since it will influence the normal earth pressure acting on the lining. Furthermore, the ground–lining interaction should be examined using in situ data.

References

AASHTO (American Association of State Highway and Transportation Officials), 2010. *Technical manual for design and construction of road tunnels – Civil elements*, p.10-14.

ACTEC (Advanced Construction Technology Center), 1999. *Manual on structural design of segmental lining with the consideration of inner water pressure*, p.86 (in Japanese).

AFTES (French Tunnelling and Underground Space Association), 2005. *Recommendation for the design, sizing and construction of precast concrete segments installed at the rear of a tunnel boring machine (TBM)*, p.232.

BSI (British Standards Institute), 2016. PAS 8810:2016: *Tunnel Design - Design of Concrete Segmental Tunnel Linings - Code of practice*. London, England.

BTS (British Tunnelling Society), 2004. *Tunnel lining design guide*. Thomas Telford Ltd., London, UK.

Chaiyaput S. and Sugimoto M., 2016. Effect of boundary conditions in segmental lining model on its sectional force. *Lowland Technology International*, 18(1), 9–22. https://doi.org/10.14247/lti.18.1_9

DAUB (Deutscher Ausschuss fur unterirdisches Bauen), 2013. *Recommendations for the design, production and installation of segmental rings*. Technical Report Deutscher Ausschuss fur unterirdisches Bauen e.V, p.23.

DIANA FEA BV, 2019. *Finite Element Analysis, User's manual*, release 10.3, 2019. Delft, The Netherlands.

Do N. A., Dias D., Oreste P., and Djeran-Maigre I., 2013. 2D numerical investigation of segmental tunnel lining behaviour. *Tunnelling and Underground Space Technology,* 37, 115–127. https://doi.org/10.1016/j.tust.2013.03.008

Do N. A., Dias D., Oreste P., and Djeran-Maigre I., 2014. A new numerical approach to the hyperstatic reaction method for segmental tunnel linings. *International Journal for Numerical and Analytical Methods in Geomechanics,* 38(15), 1617–1632. https://doi.org/10.1002/nag.2277

Duddeck H. and Erdman J., 1985. On structural design models for tunnels in soft soil. *Underground Space,* 9, 246–259. Pergamon Press, Oxford, UK.

Duddeck, H., 1980. Empfehlungen zur Berechnung von Tunneln im Lockergestein. *Die Bautechnik*, 57, 349–356 (in German).

Einstein H. H. and Schwartz C. W., 1979. Simplified Analysis for Tunnel Supports. *Journal of the Geotechnical Engineering Division*, 105, 499-517.

El-Nahhas F., El-Kadi F., and Ahmed A., 1992. Interaction of tunnel linings and soft ground. *Tunnelling and Underground Space Technology*, 7(1), 33–43. https://doi.org/10.1016/0886-7798(92)90111-T

Fujii K., Mashimo H., Ishimura T., and Mayumi H., 1999. Prediction of ground movement due to shield tunneling. *Proc. of Tunnel Engineering, JSCE*, 9, 243–248 (in Japanese).

Hofmann M., Cordes T., Bergmeister K., 2019. The subgrade reaction modulus method in tunnelling. *Proceedings of the WTC 2019 ITA-AITES World Tunnel Congress (WTC 2019)*, May 3-9, 2019, Naples, Italy

Ishigaki H., Sawakami S., Mori M., and Hattori Y., 2016. An Experimental Study on Design Method for Segment Joint of Shield Tunnel which is Subject to High Tensile Force. *Journal of Japan Society of Civil Engineers*, 72(3), 136-149.

ITA (International Tunnelling Association), 2000. Guidelines for the design of shield tunnel lining. *Tunnellingand Underground Space Technology*, 15(3), 303–331. https://doi.org/10.1016/S0886-7798(00)00058-4

Itasca Consulting Group, Inc., 2016. *Fast Lagrangian Analysis of Continua, User's guide*, version 5.1.

JSCE (Japan Society of Civil Engineers), 2016. *Standard specifications for tunneling-2016: shield tunnels*.

Kimura S., Kanda H., Nanmoku T., Koizumi A., 2002. Applicability of the beam-spring model with ground springs set all around the lining to design of shield tunnel lining by comparison of in-situ measurements and the sensitivity analysis. *Journal of Japan Society of Civil Engineers*, 721, 119–138 (in Japanese).

Kojima S., Hashimoto M., and Nagaya J., 2002. In-site measurement on earth pressure acing on segment of underground river tunnel. *Proc. of Tunnel Engineering, JSCE*, 12, 501–506 (in Japanese). https://doi.org/10.11532/journalte1991.12.501

Koyama Y. and Nishimura T., 1997. The design of lining segment of shield tunnel using a spring model with two ring beams. *Proc. of Tunnel Engineering, JSCE*, 7, 279-284 (in Japanese). https://doi.org/10.11532/journalte1991.7.279

Kuesel, Thomas R., King, Elwyn H., Bickel, John O., 1996. *Tunnel Engineering Handbook*. Kluwer Academic Publishers, Massachusetts, USA, p.87.

Mashimo H. and Ishimura T., 2005. Numerical modelling of the behavior of shield tunnel lining during assembly of a tunnel ring. *Proc., 5th Int. Symp. on Geotechnical Aspects of Underground Construction in Soft Ground*, Taylor & Francis, Amsterdam, The Netherlands, 587–593.

Matsumoto Y. and Nishioka T., 1991. *Theoretical tunnel mechanics*. University of Tokyo Press, Tokyo, Japan, p.178.

Molins C. and Arnau O., 2011. Experimental and analytical study of the structural response of segmental tunnel linings based on an in situ loading test. Part 1: Test configuration and execution. *Tunnelling and Underground Space Technology*, 26, 764–777. https://doi.org/10.1016/j.tust.2011.05.002

Morgan H., 1961. A contribution to the analysis of stress in a circular tunnel. *Geotechnique*, 11(1), 37–46. https://doi.org/10.1680/geot.1961.11.1.37

45

Muir Wood A. M., 1975. The circular tunnel in elastic ground. *Geotechnique*, 25, 115–127. https://doi.org/10.1680/geot.1975.25.1.115

Nematollahi M., Dias D., 2019. Three-dimensional numerical simulation of pile-twin tunnels interaction-Case of the Shiraz subway line. *Tunnellingand Underground Space Technology*, 86(2019), 75–88. https://doi.org/10.1016/j.tust.2018.12.002

OVBB (Austrian Association for Concrete and Construction Technology), 2011. *Guideline Concrete segmental lining systems*. Austrian Society for Concrete and Construction, p.18.

Plizzari G. A. and Tiberti G., 2006. Steel fibers as reinforcement for precast tunnel segments. *Tunnelling Underground Space Technology*, 21(3), 438–439. https://doi.org/10.1016/j.tust.2005.12.079

RTRI (Railway Technical Research Institute), 1997. *Design standards for railway structures and commentary (Shield tunnel)*. Maruzen, Tokyo, Japan, p. 60 (in Japanese).

Schulze, H., and Duddeck, H., 1964. Spannungen in schildvorgetriebenen tunneln. *Beton-und Stahlbetonbau*, 59(8), 169–175.

Sramoon A., and Sugimoto M., 2000. Development of ground reaction curve for shield tunnelling. *Proc. Int. Symp. on Geotechnical Aspects of Underground Construction in Soft Ground, Balkema, The Netherlands*, 431–436.

Sugimoto M., Asanprakit A., 2010. Stack pipe model for pipe jacking method. *Journal of Construction Engineering and Management*, 136(6), 683–692

Sugimoto M., Chen J., Sramoon A, 2019. Frame structure analysis model of tunnel lining using nonlinear ground reaction curve. *Tunnelling Underground Space Technology*, 94(2019), 1–7

Sugimoto M., Sramoon A., 2002a. Theoretical model of shield behavior during excavation: I. Theory. *Journal of Geotechnical and Geoenvironmental Engineering*, 128(2), 138–155

Sugimoto M., Sramoon A., and Okazaki M., 2011. Tunnel lining design method by frame structure analysis using ground reaction curve. *Journal of Japan Society of Civil Engineers*, Division C, 67(1), 61–77 (in Japanese). https://doi.org/10.2208/jscejge.67.61

Sugimoto M., Sramoon A., Kayukawa K., 2002b. Theoretical model of shield behavior during excavation. II: Application. *Journal of Geotechnical and Geoenvironmental Engineering*, 128(2), 156–165

Sugimoto M., Sramoon A., Konishi S., Sato Y., 2007. Simulation of shield tunneling behavior along a curved alignment in a multilayered ground. *Journal of Geotechnical and Geoenvironmental Engineering*, 133(6), 684–694

Thienert C. and Pulsfort M., 2011. Segment design under consideration of the material used to fill the annular gap. *Geomechanics and Tunnelling,* 4(6), 665–679. https://doi.org/10.1002/geot.201100050

Vitali O. P. M., Celestino T. B., and Bobet A., 2018. 3D finite element modelling optimization for deep tunnels with material nonlinearity. *Underground Space*, 3(2), 125–139. https://doi.org/10.1016/j.undsp.2017.11.002

Vu M. N., Broere W., Bosch J. W., 2017. Structural analysis for shallow tunnels in soft soils. *International Journal of Geomechanics* 17(8). https://doi.org/10.1061/(ASCE)GM.1943-5622.0000866

Yamada K., Yoshida T., Magata H., and Hashimoto S., 1986. Behavior of ground displacement due to shield thrusting in alluvial subsoils and its prediction analysis. *Journal of Japan Society of Civil Engineers*, 272, 103–112 (in Japanese). https://doi.org/10.2208/jscej.1986.373_103

Zhang D., Huang H., Phoon K. K., Hu Q., 2014. A modified solution of radial subgrade modulus for a circular tunnel in elastic ground. *Soils and Foundations*, 54(2), 225-232.

Zhang Z., Zhang M., Jiang Y., Bai Q., and Zhao Q., 2017. Analytical prediction for ground movements and liner internal forces induced by shallow tunnels considering non-uniform convergence pattern and ground-liner interaction mechanism. *Soils and Foundations*, 57, 211–226. https://doi.org/10.1016/j.sandf.2017.03.004

Tables:

Table 2.1. Stiffness of tangential spring between ground and lining.

Value	References
$k_t \cong 0$	Duddeck, 1980; Matsumoto and Nishioka, 1991; RTRI, 1997; Koyama and Nishimura, 1997; AASHTO, 2010; DAUB, 2013; OVBB, 2011; Sugimoto et al., 2011
$k_t = k_n/3$	RTRI, 1997; Koyama and Nishimura, 1997; Mashimo and Ishimura, 2005; JSCE, 2016; Plizzari and Tiberti, 2006; Molins and Arnau, 2011
$k_t = k_n$	Do et al., 2013; Itasca, 2016; Nematollahi and Dias, 2019

Note: k_t is the tangential spring constant per unit area. k_n is the normal spring constant at the crown point.

Table 2.2. Test on segment joint type

Type no.	Type		Segment thickness (mm)	Joint type
1	A-A		300	Metal fittings
2			300	Ductile fittings
3			400	Metal fittings
4			550	Core type
5	B-K-B	Radial insertion type	300	Metal fittings
6		Axial insertion type	300	Metal fittings

Table 2.3. Rotational spring constant of test type

	Axial force (kN)	Type no.	Rotational spring constant (kN.m/rad)					
			1	2	3	4	5	6
Positive moment	0	k_{m1}	17000	43400	48800	30000	18200	48800
		k_{m2}	-	22300	35800	63700	-	35800
		k_{m3}	-	17100	-	-	-	-
	500	k_{m1}	69800	128600	134400	139200	77700	134400
		k_{m2}	21900	64200	87100	99000	30900	87100
		k_{m3}	-	31200	53500	66800	22100	53500
	1500	k_{m1}	329500	299500	417100	297100	226000	417100
		k_{m2}	149100	190700	175400	175600	84700	175400
		k_{m3}	63900	145600	85200	77800	-	85200
Negative moment	0	k_{m1}	6800	53400	40600	54800	37800	67900
		k_{m2}	11200	28600	17600	32700	18600	28200
		k_{m3}	-	20900	-	28600	11000	13500
	500	k_{m1}	67900	137200	180800	105300	121000	161000
		k_{m2}	38300	65500	67800	69400	57800	78400
		k_{m3}	19000	30200	29900	38400	24600	29000
	1500	k_{m1}	342800	305600	878600	452700	242000	442000
		k_{m2}	142500	174600	358900	222500	125000	231000
		k_{m3}	75700	84000	160500	124100	-	-

Table 2.4. Coefficient of subgrade reaction for various types of ground

Treatment of soil and groundwater	Ground condition	k (MN/m³)	Approximate N-value
Effective stress method	Very dense sandy soil	30 - 50	30 < N
	Medium dense sandy soil	10 - 30	15 < N < 30
	Loose sandy soil	0 - 10	N < 15
	Hard cohesive soil	30 - 50	25 < N
	Stiff cohesive soil	10 - 30	8 < N < 25
	Medium stiff cohesive soil	5 - 10	4 < N < 8
Total stress method	Medium stiff cohesive soil	5 - 10	4 < N < 8
	Soft cohesive soil	0 - 5	2 < N < 4
	Very soft cohesive soil	0	N < 2

Table 2.5. Analysis cases of parameter study.

Case	k_t/k_n	Load model	Coefficient of subgrade reaction, MN/m³	Overburden depth, m
10	0	Type 0 (no τ_0)	10, 50, 100, 500, 1000	7.870, 37.635
20	1/3			
30	1			
11	0	Type 1 (with τ_0)		
21	1/3			
31	1			

Table 2.6. Segmental lining dimensions and material properties.

Radius (m)	3.935
Thickness (m)	0.370
Width (m)	1.000
Density (kN/m³)	28.000
Elastic modulus (GN/m²)	33
Poisson ratio	0.2
Segment joint spring, k_θ (MNm/rad)	35.4
Ring joint spring in normal dir., k_{sr} (MN/m)	827
Ring joint spring in shear dir., k_{st} (MN/m)	1260

Table 2.7. Tunnel position and ground properties.

Ground properties	Deep tunnel	Shallow tunnel
Overburden depth (m)	37.635	7.870
Groundwater level (m)	GL-7.126	GL-7.126
Submerged density (kN/m³)	5.500	5.500
Vertical effective earth pressure at crown (kN/m²)	342.27	127.84
Water pressure at crown (kN/m²)	300.80	9.10
Coef. of earth pressure $K_{h\,min}$, K_{h0}, $K_{h\,max}$	0.0 , 0.5 , 5.0	0.0 , 0.5 , 5.0
Coef. of earth pressure $K_{v\,min}$, K_{v0}, $K_{v\,max}$	0.0 , 1.0 , 5.0	0.0 , 1.0 , 5.0

Figures:
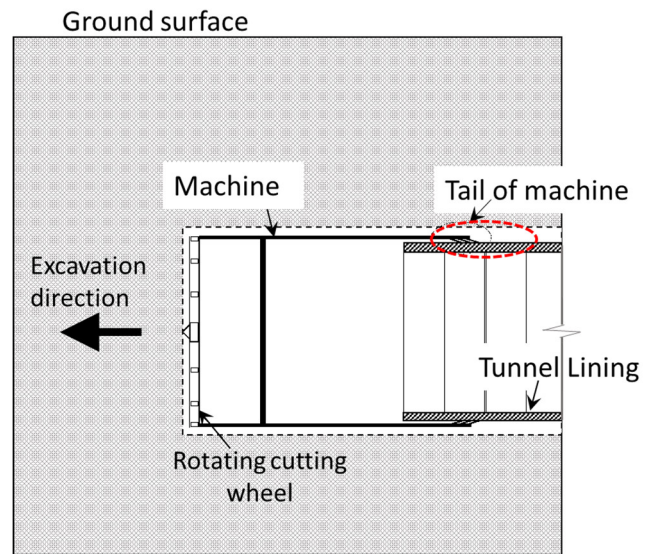
Figure 1.1. Concept of shield tunneling method.
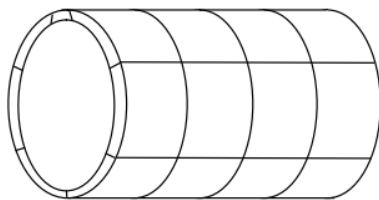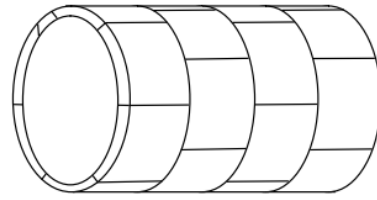
a) Straight joint   b) Staggered arrangement

Figure 1.2. Connections of segments and configuration of staggered joints.
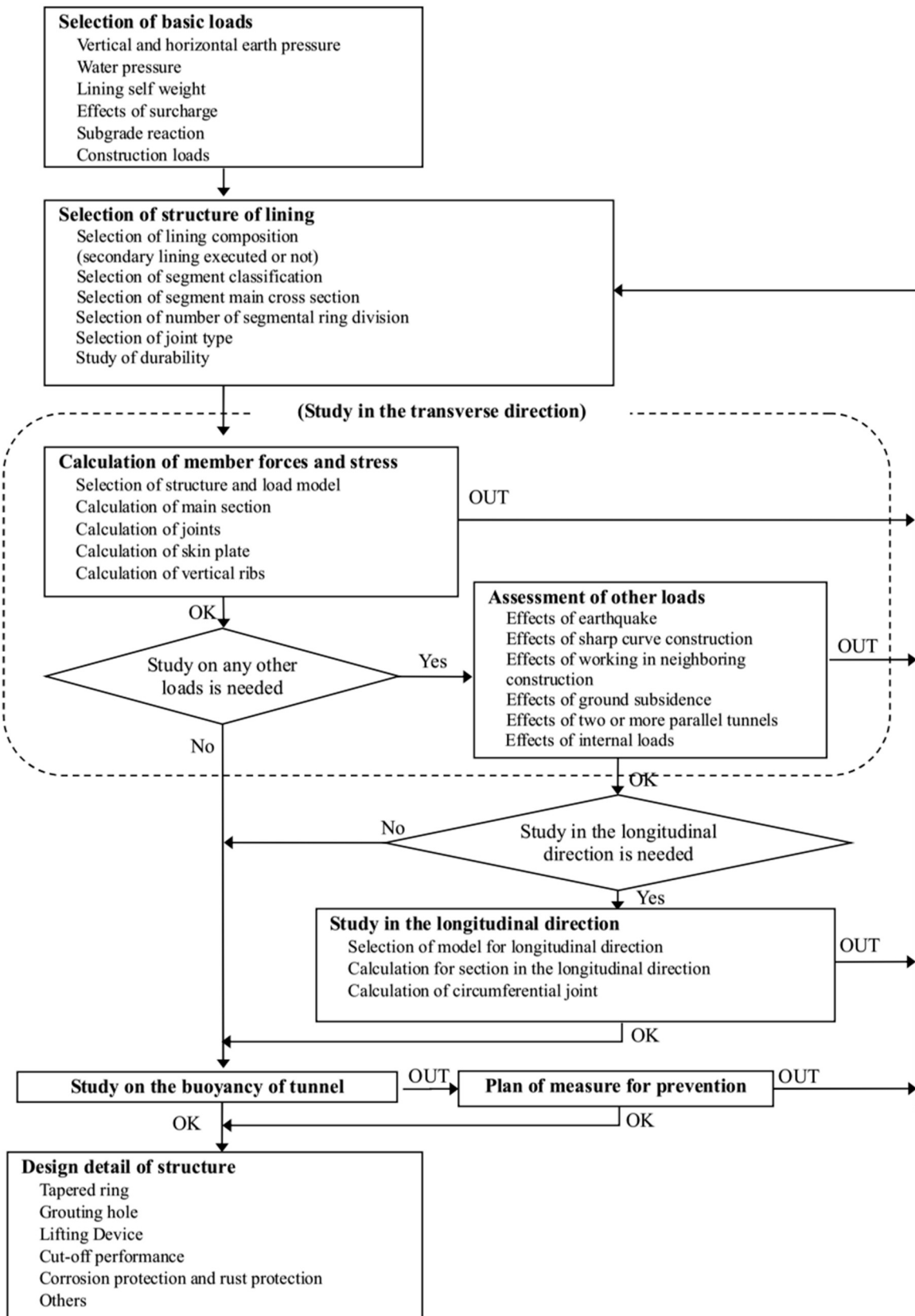
Figure 1.3. Flow chart for the tunnel lining structure design.
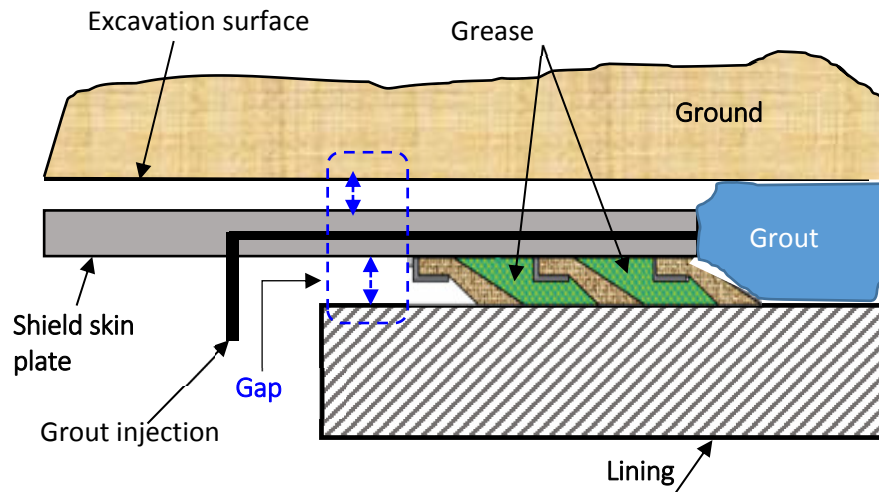
Figure 1.4. Gap between the lining and surrounding ground.

Figure 2.1. Coating outer surface of segments.
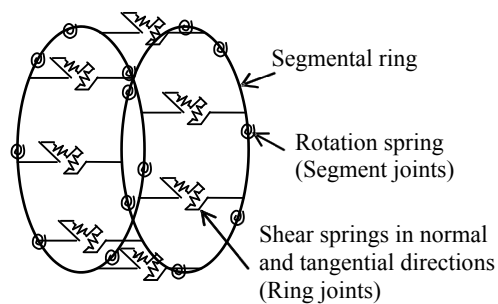
Figure 2.2. Beam-spring model.
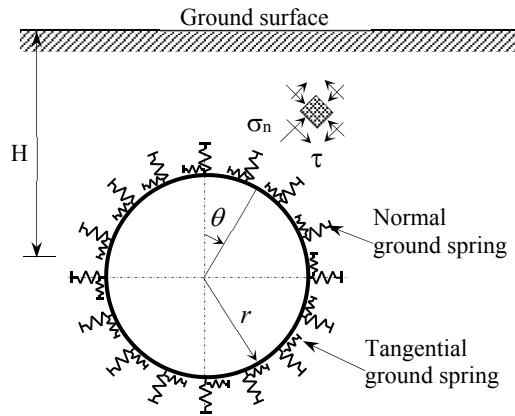
Figure 2.3. Ground pressure and ground springs around the lining.

a) Type 0: Normal earth pressure

b) Type 1: Vertical and horizontal earth pressure

Figure 2.4. Load models for the lining analysis.
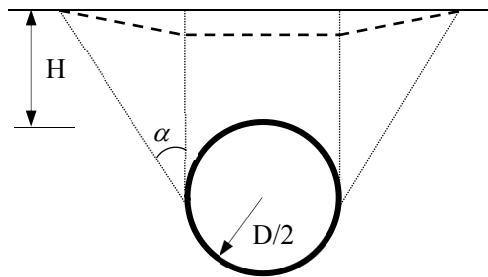
Figure 2.5. Ground surface settlement profile in case of shallow tunnel.

a) Buoyancy   b) Vertical deformation

c) Earthquake effect
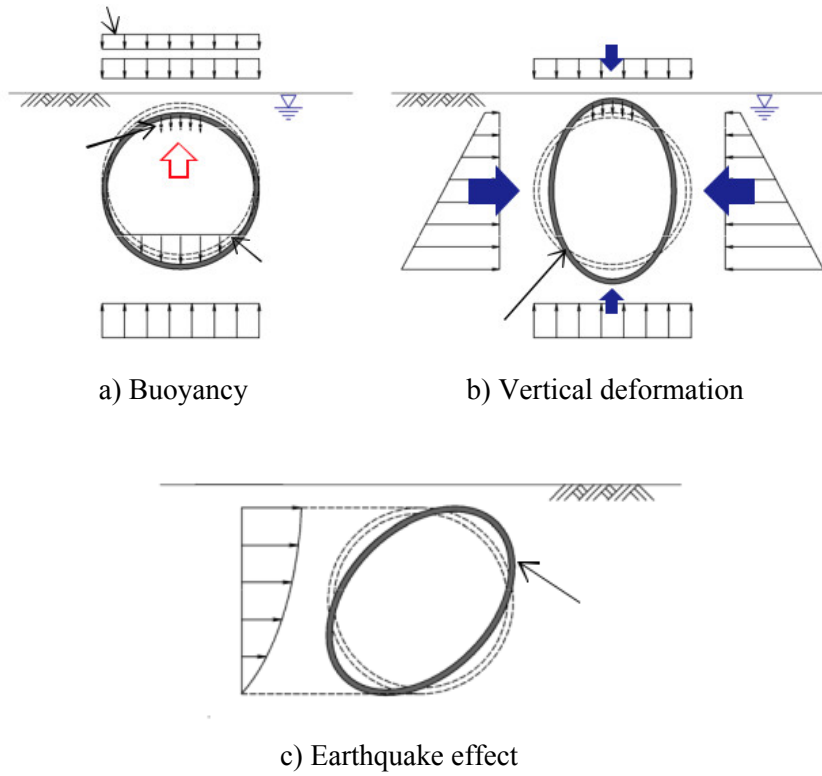
Figure 2.6. Design problems of shallow tunnel.
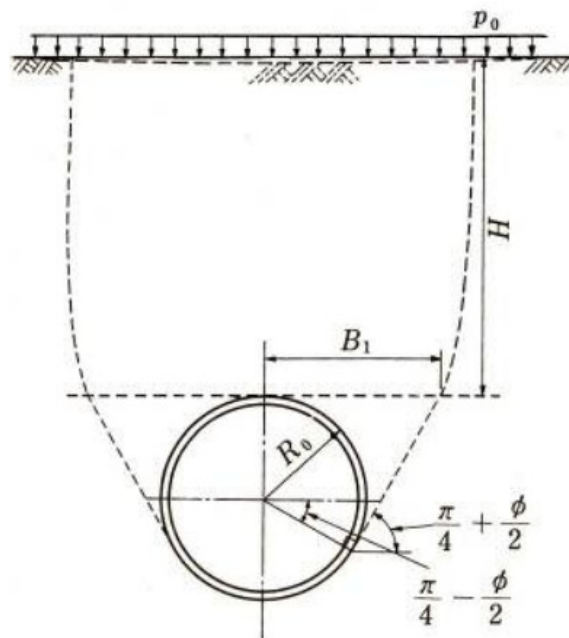
Figure 2.7. Loosening earth pressure calculation.
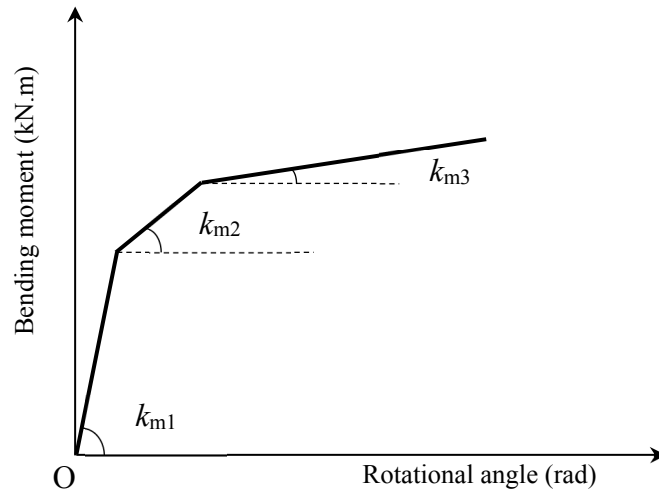
Figure 2.8. Relationship between bending moment and rotational angle.
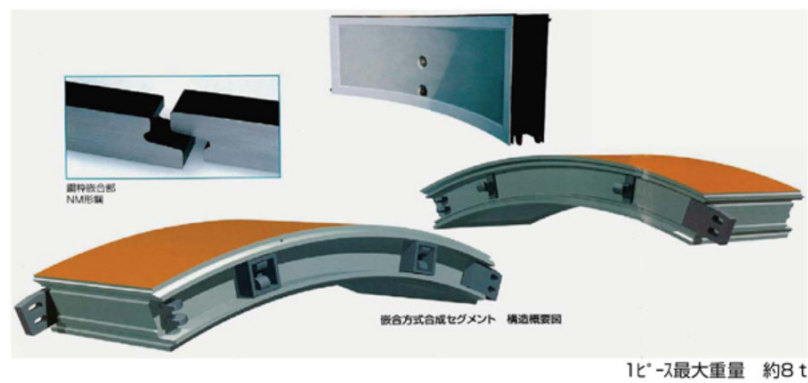
Figure 2.9. Segment shape and connection method.

Source: https://kozobutsu-hozen-journal.net/interviews/detail.php?id=1106&page=2
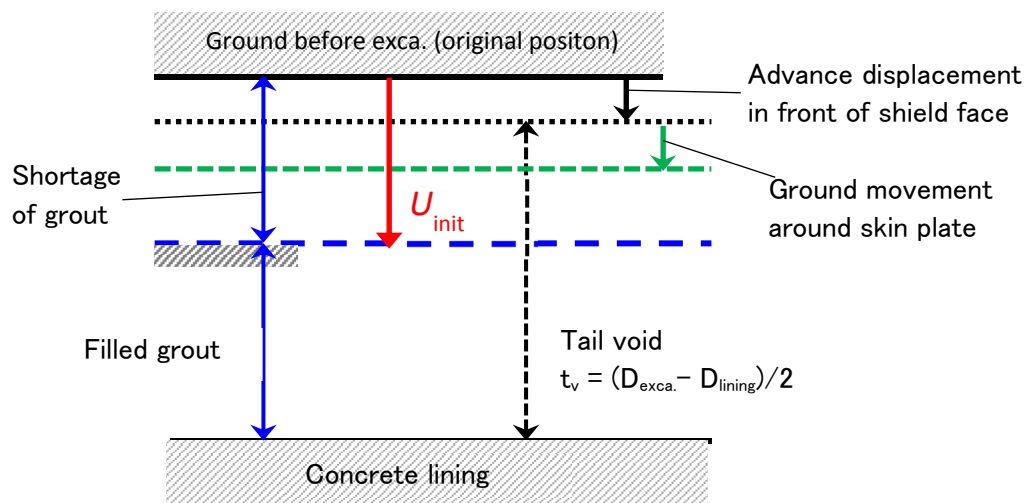
Figure 2.10. Factors influencing the interaction.
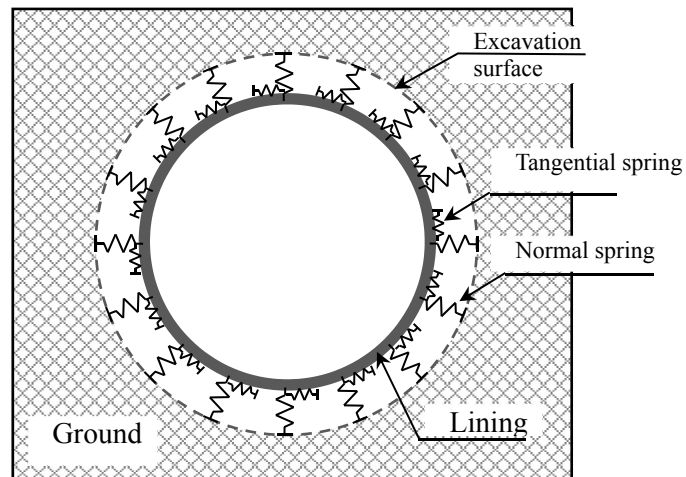
Figure 2.11. Interaction springs between lining and ground.
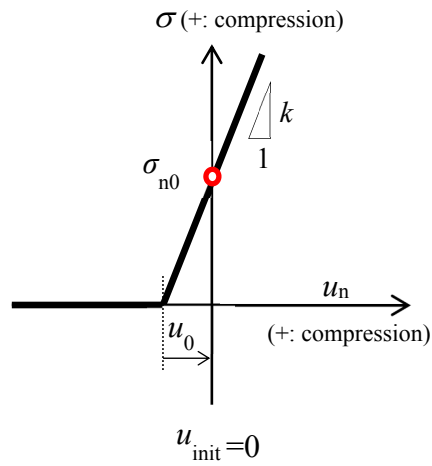
Figure 2.12. Normal spring model in case of $u_{init} = 0$.
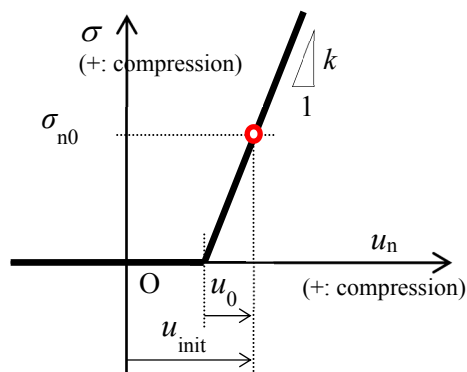
Figure 2.13. Normal spring model in case of $u_{init} < 0$.
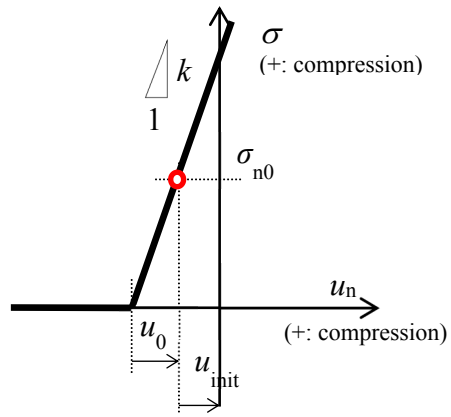
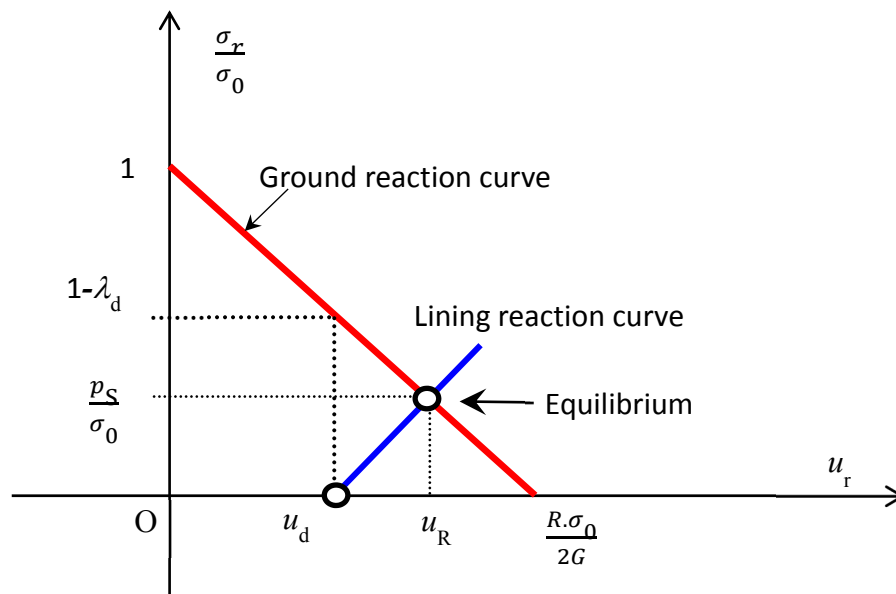**Figure 2.14.** Normal spring model in case of $u_{\text{init}} > 0$.
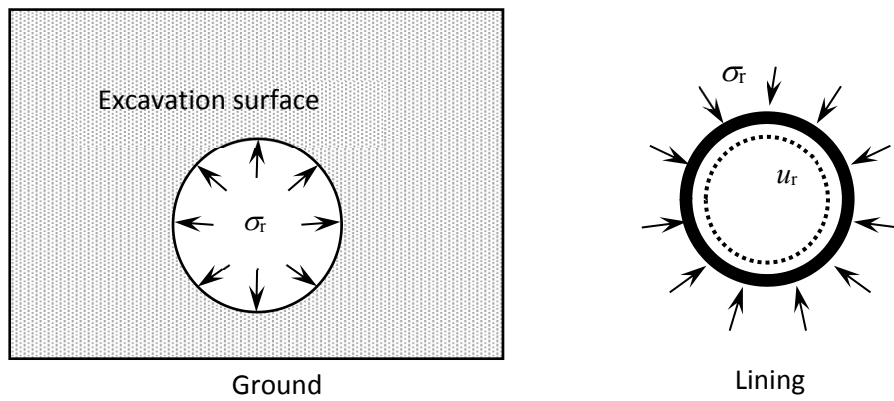
a) Pressure on lining and ground, and displacement of ground.

b) The interaction explanation

Figure 2.15. Convergence-confinement method.

Note: $\sigma_r = 0$ with $u_r = R.\sigma_0/(2G)$ when there is no support, where R is tunnel radius, G is shear modulus of linear elastic soil.
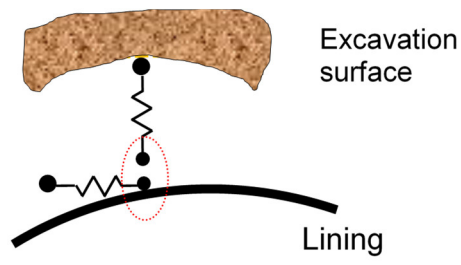
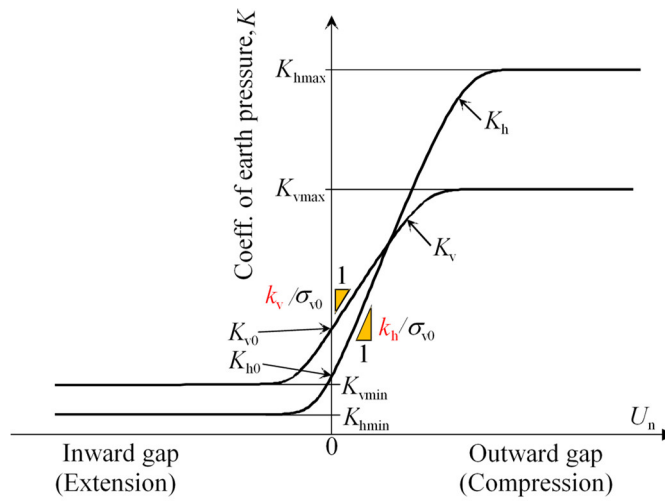**Figure 2.16.** Ground-lining interaction by spring elements.

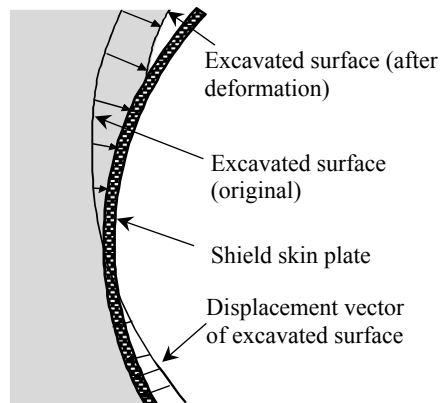

Figure 2.17. Ground reaction curves.

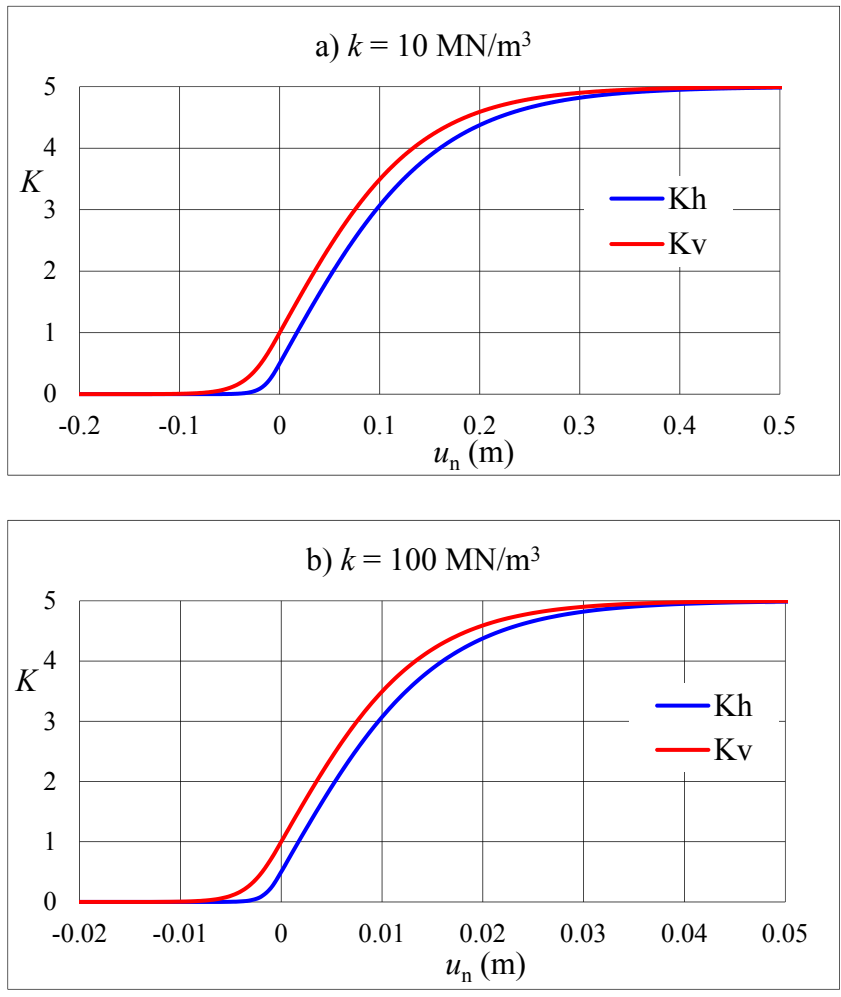**Figure 2.18**. Displacement of excavated surface.

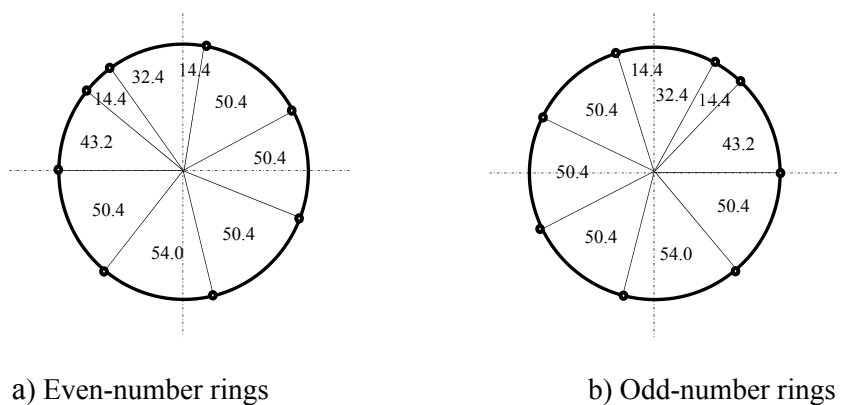**Figure 2.19.** Ground reaction curves for several types of ground.

a) Even-number rings   b) Odd-number rings

Figure 2.20. Staggered arrangement of segments.
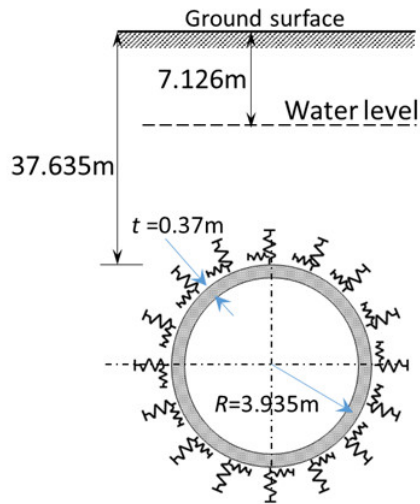
Figure 2.21. Tunnel location and underground water level.

a) Deep tunnel   b) Shallow tunnel

c) Directions of initial normal and shear forces acting on lining ($K_{h0} < 1$)

——— Effective normal earth pressure

----- Tangential earth pressure
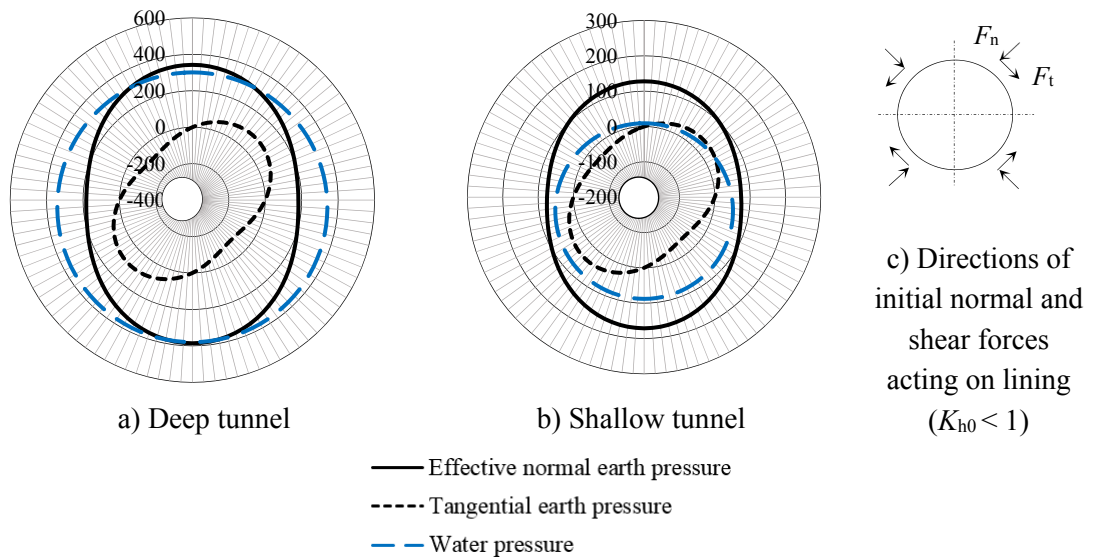
— — Water pressure

Figure 2.22. Distribution of initial earth pressure and water pressure on lining (kN/m²).
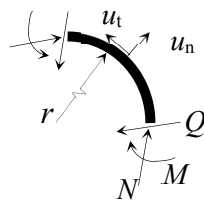
Figure 2.23. Sign convention for sectional forces, normal and tangential displacement.
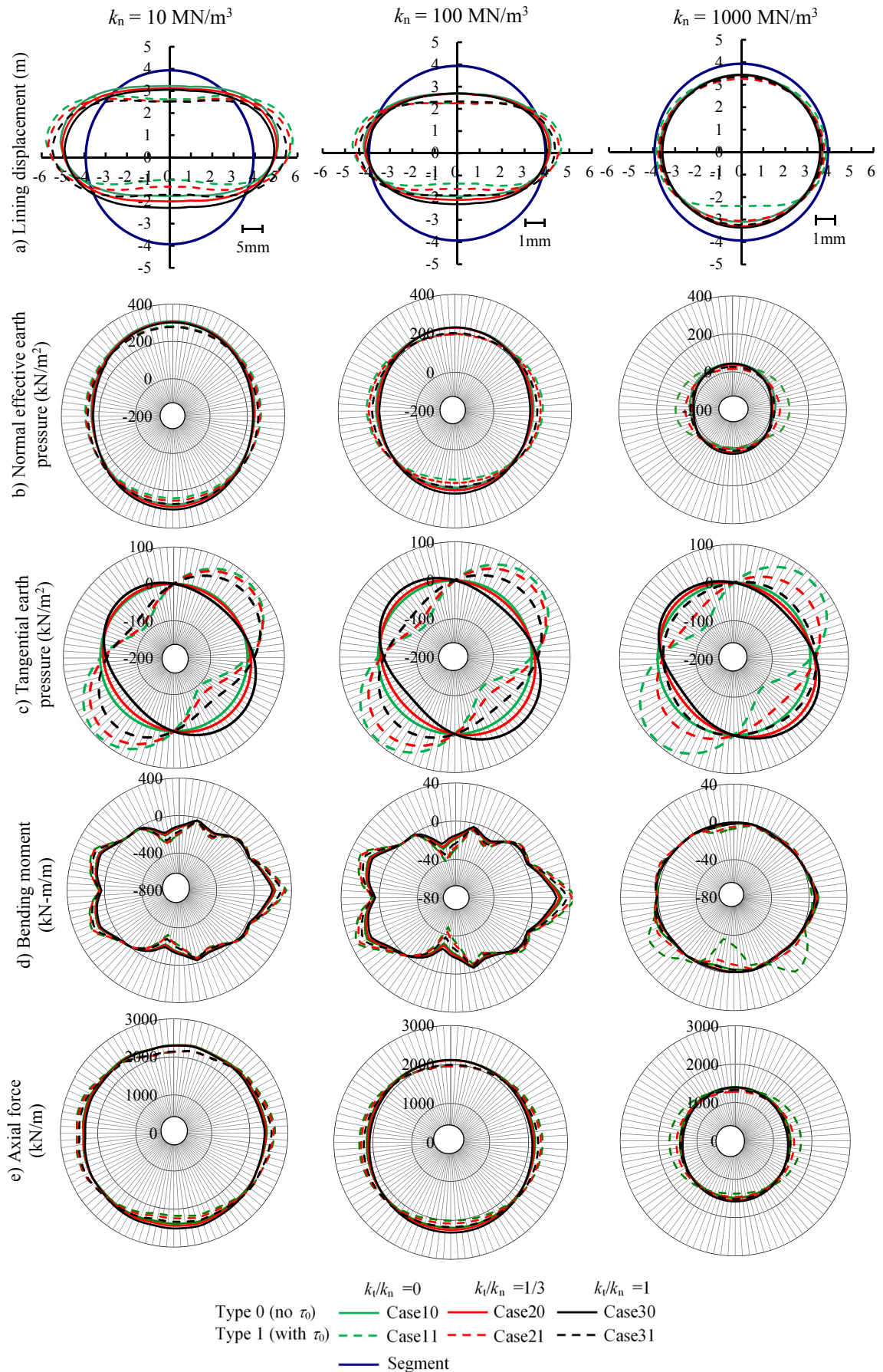
Figure 3.1. Lining displacement and ground reactions (deep tunnel).
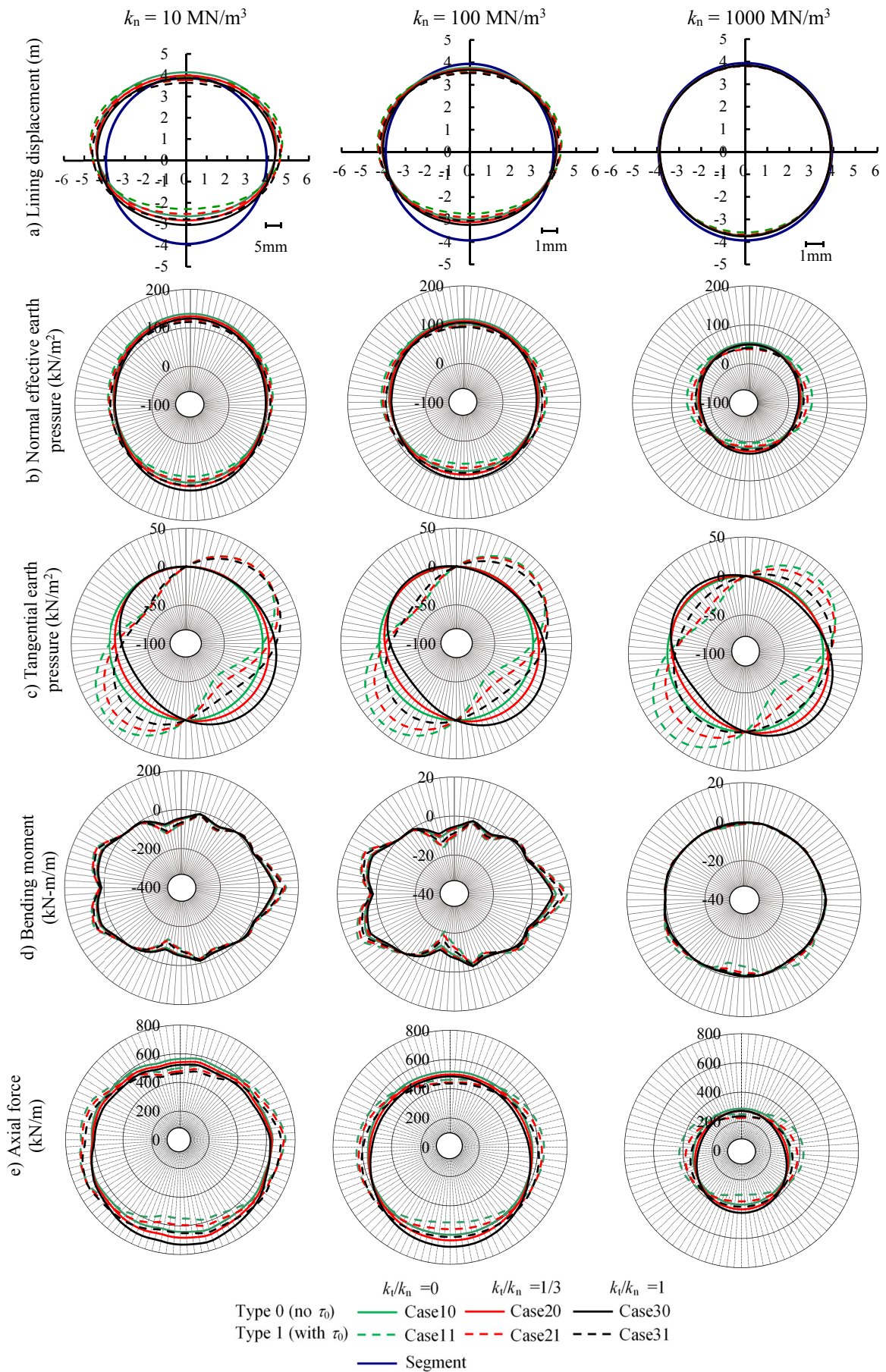
Figure 3.2. Lining displacement and ground reactions (shallow tunnel).

64
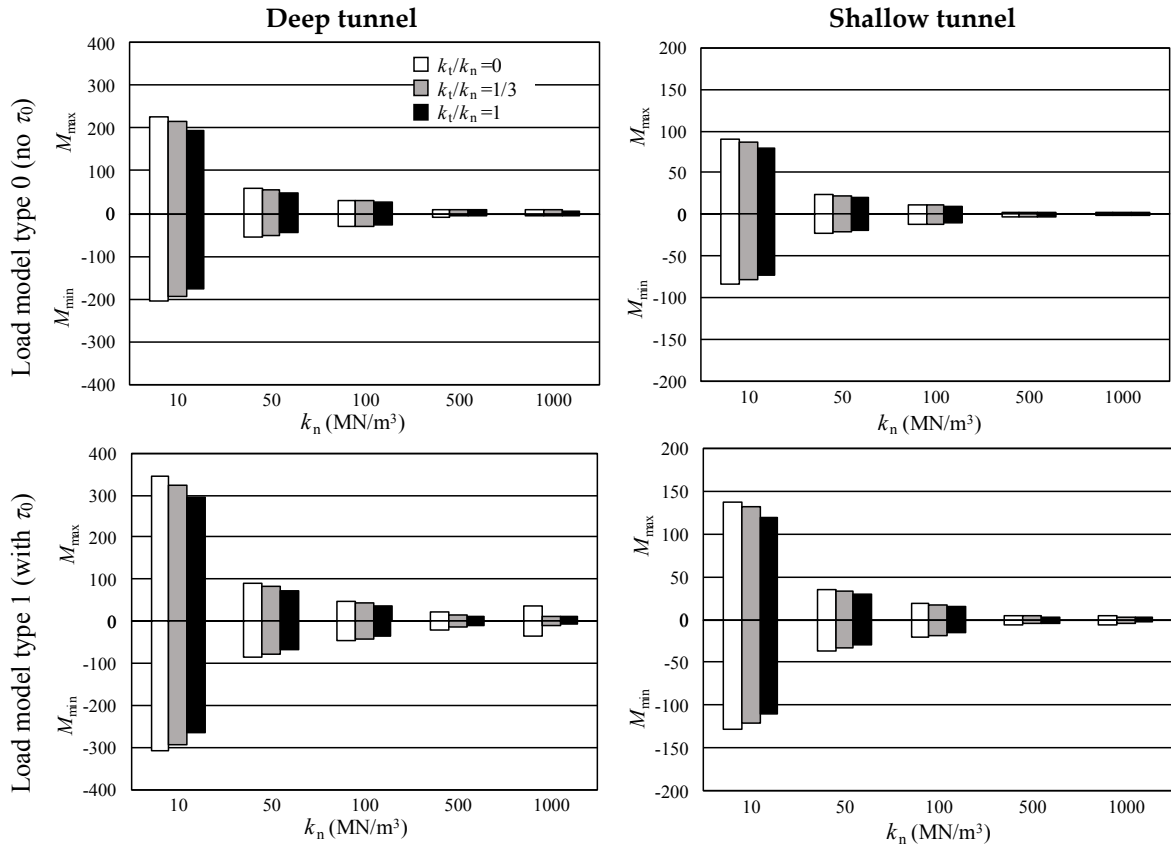
Figure 3.3. Maximum and minimum bending moment (kN-m/m).

(**a**)　　　　　　　　　　　　　　　(**b**)
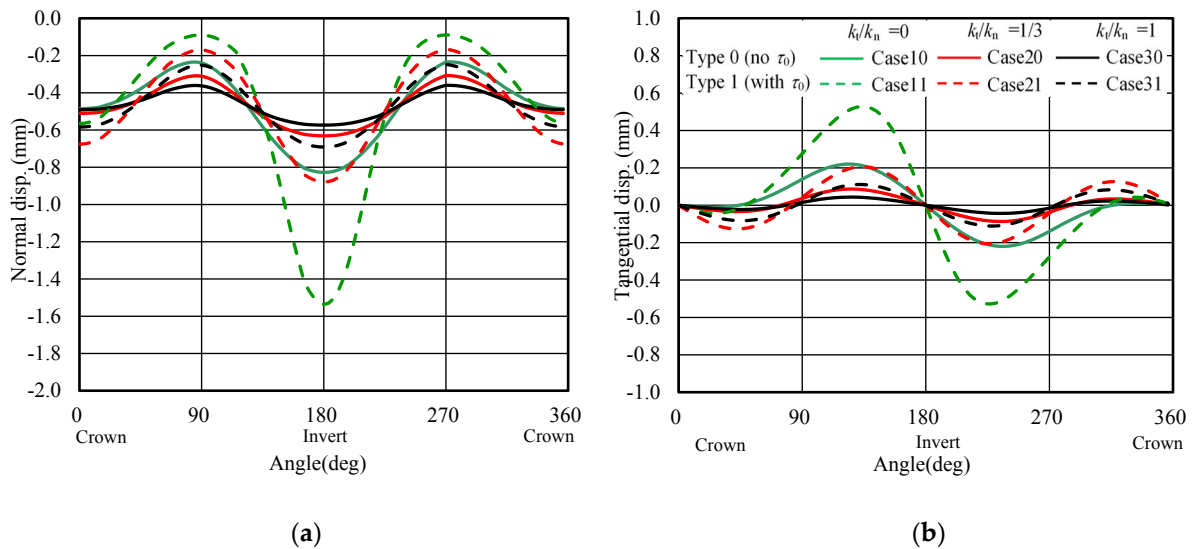
Figure 3.4. Lining displacement for ground at k_n =1000 MN/m³ (deep tunnel). (**a**) Normal displacement (+: outward); (**b**) Tangential displacement (+: counterclockwise)
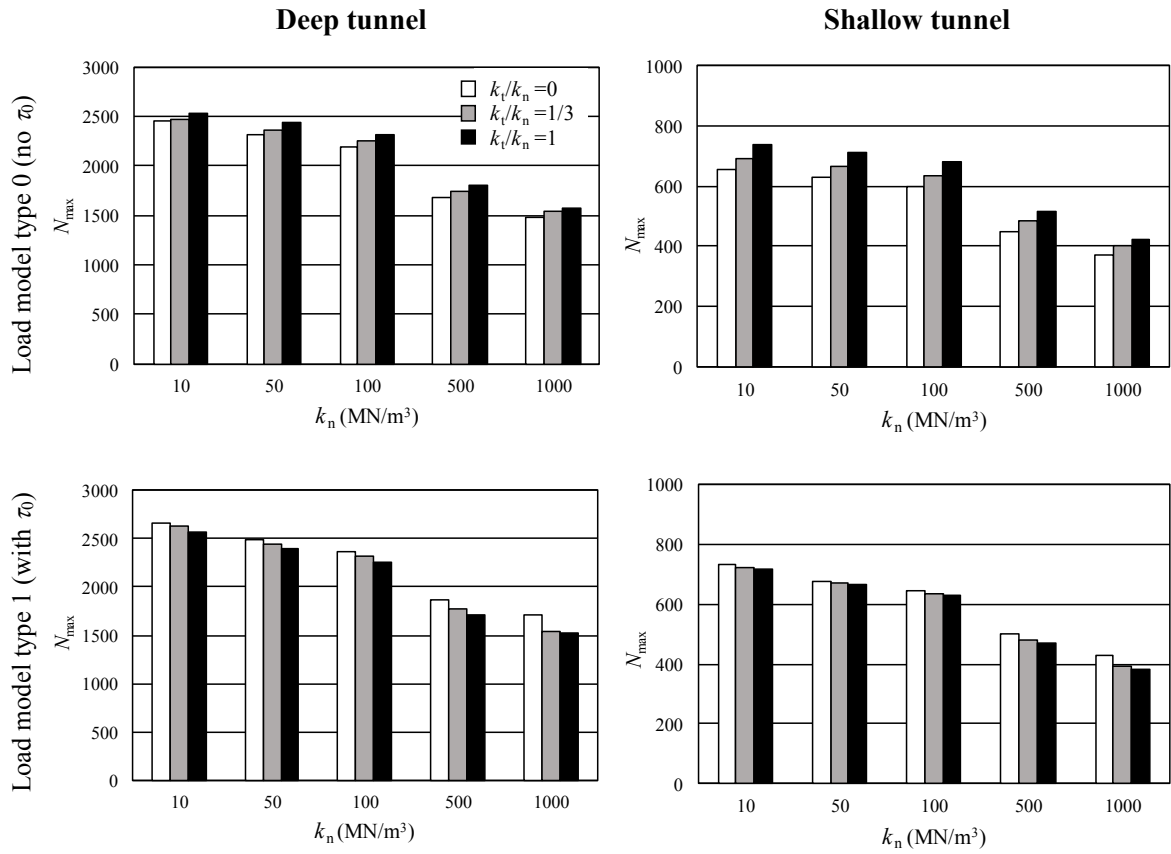
Figure 3.5. Maximum axial force (kN/m).
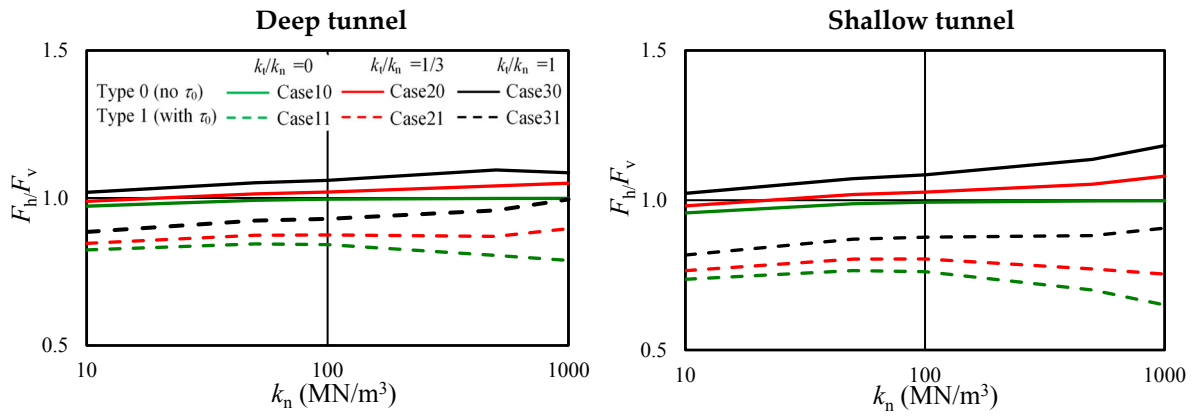
Figure 3.6. F_h/F_v.
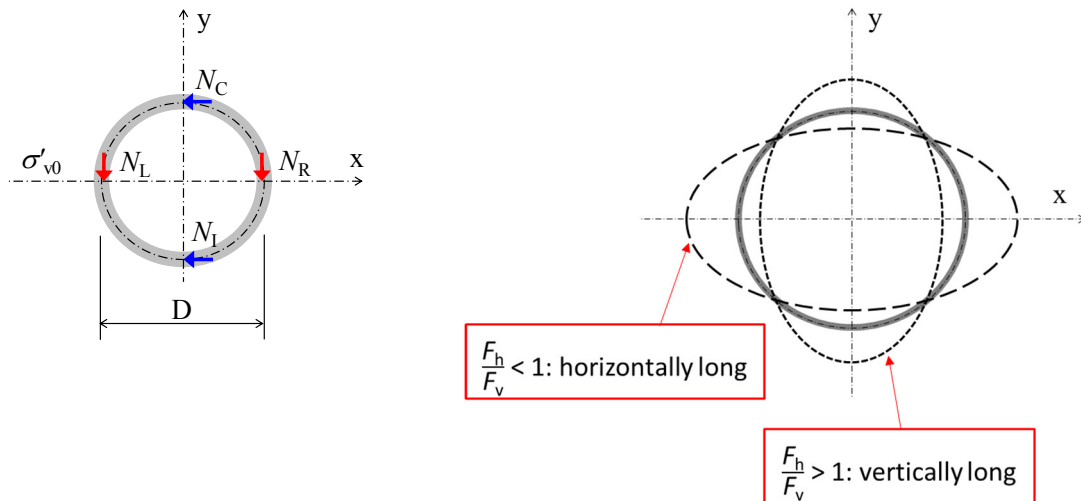
Figure 3.7. Shape of axial force distribution.
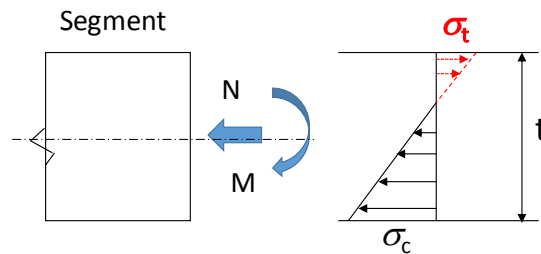
Figure 3.8. Tensile stress in the segment.
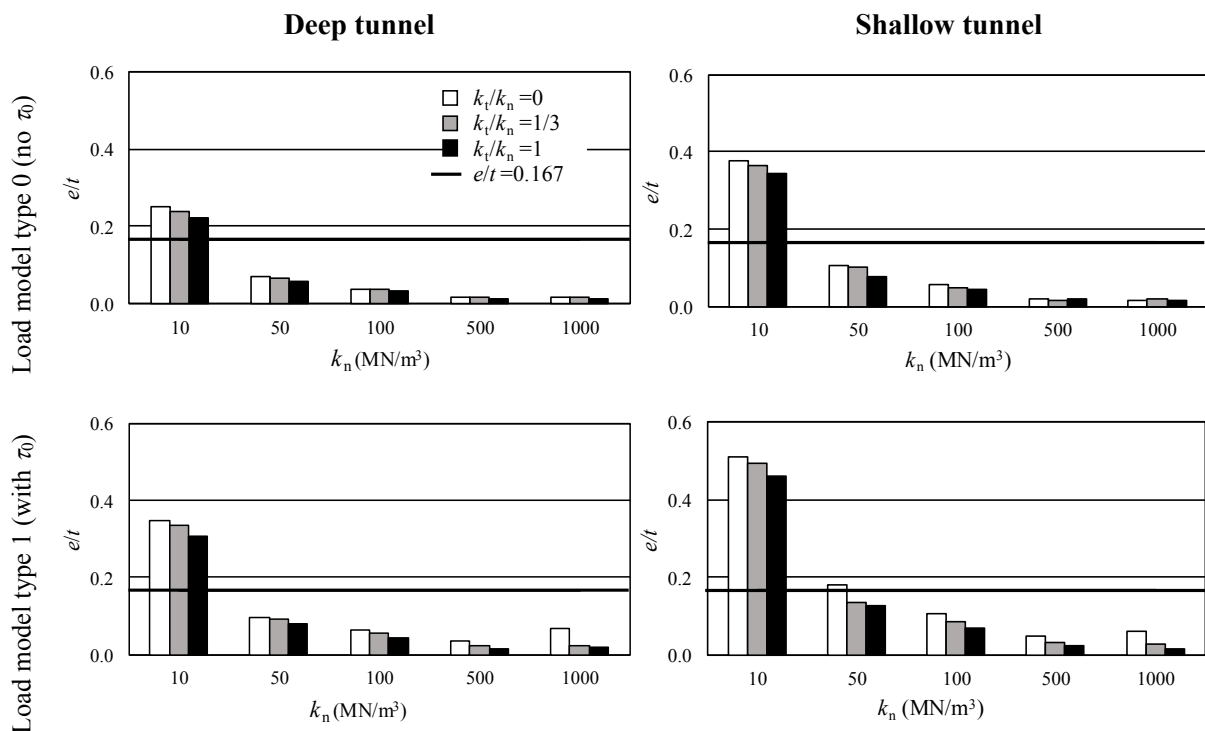
Figure 3.9. Normalized eccentricity.

67

Deep tunnel　　　　　　　　　　　　　　**Shallow tunnel**
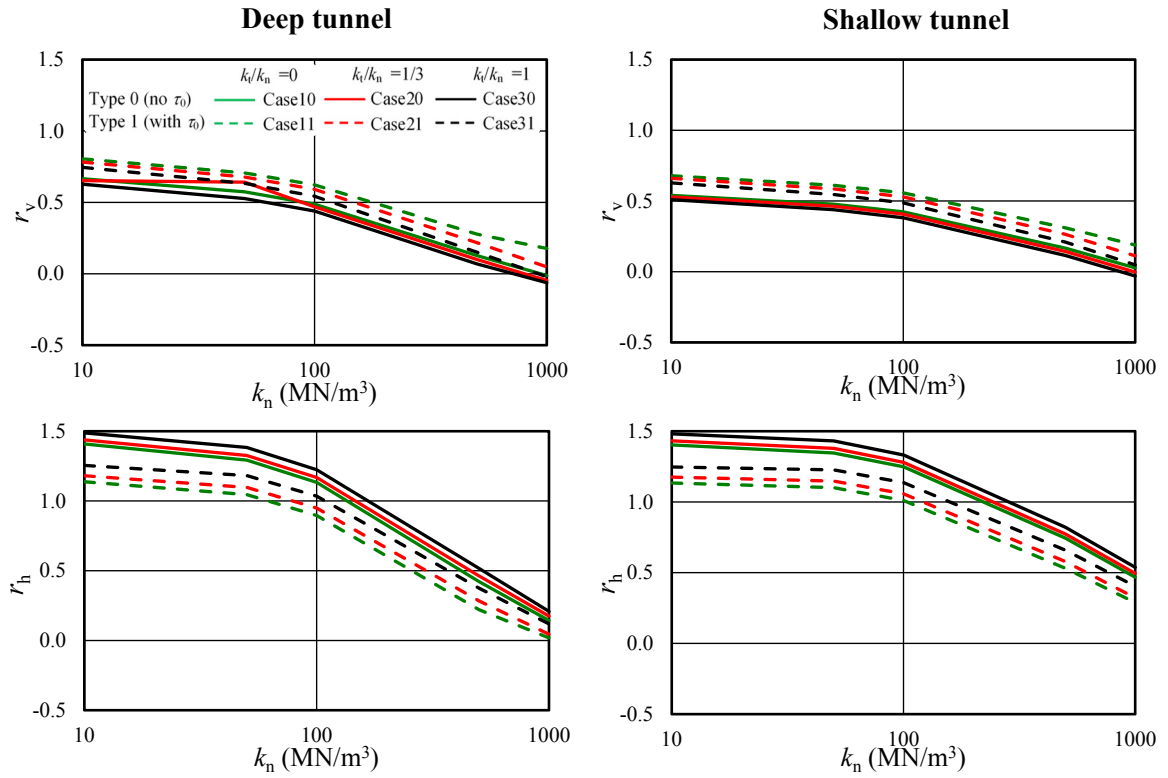
Figure 3.10. Support rate of initial effective earth pressure by lining in the vertical and horizontal direction r_v, r_h.
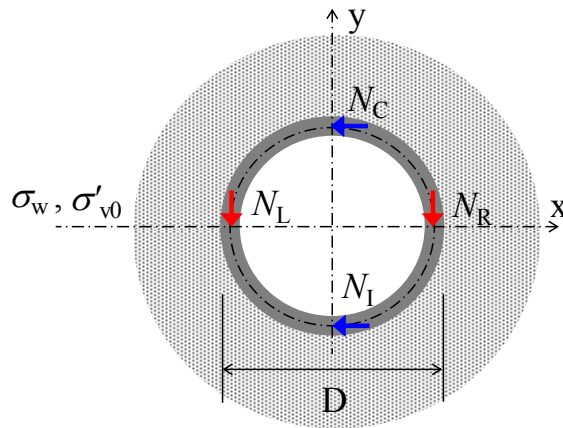
Figure 3.11. Axial forces in the lining at the left and right spring lines, crown, and invert.

Appendix

Appendix A. Lining behaviour for k = 50 MN/m³ and k = 500 MN/m³

Appendix B. Data for building M, N, e/t graphs

Appendix A. Lining behaviour in ground $k = 50$ and $k = 500$ MN/m³

k = 50 MN/m^3	k = 500 MN/m^3

Lining disp. (m)

2mm

1mm

Effective earth pressure (kPa)

Tangential earth pressure (kPa)

Bending moment (kN-m)

Axial force (kN)
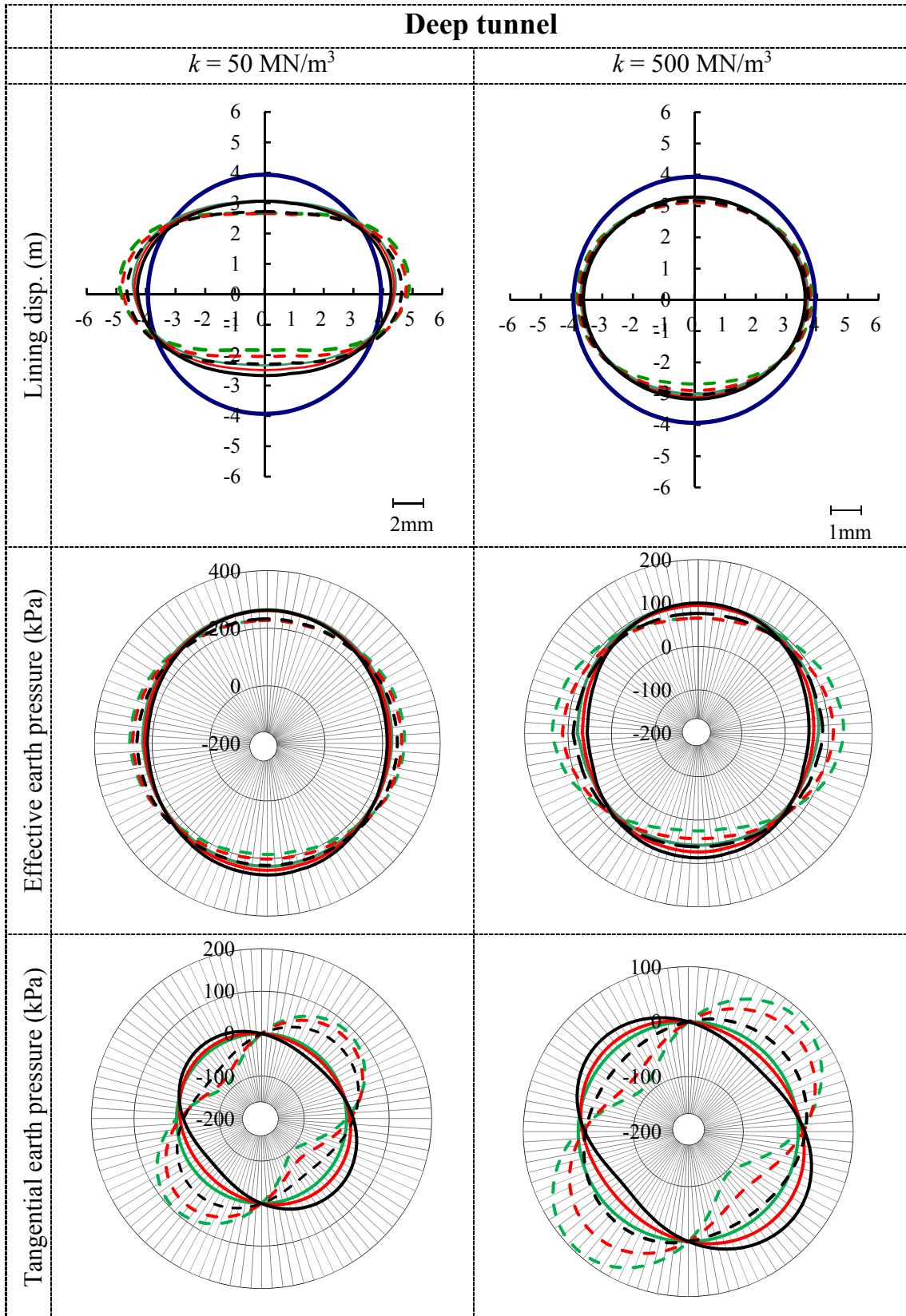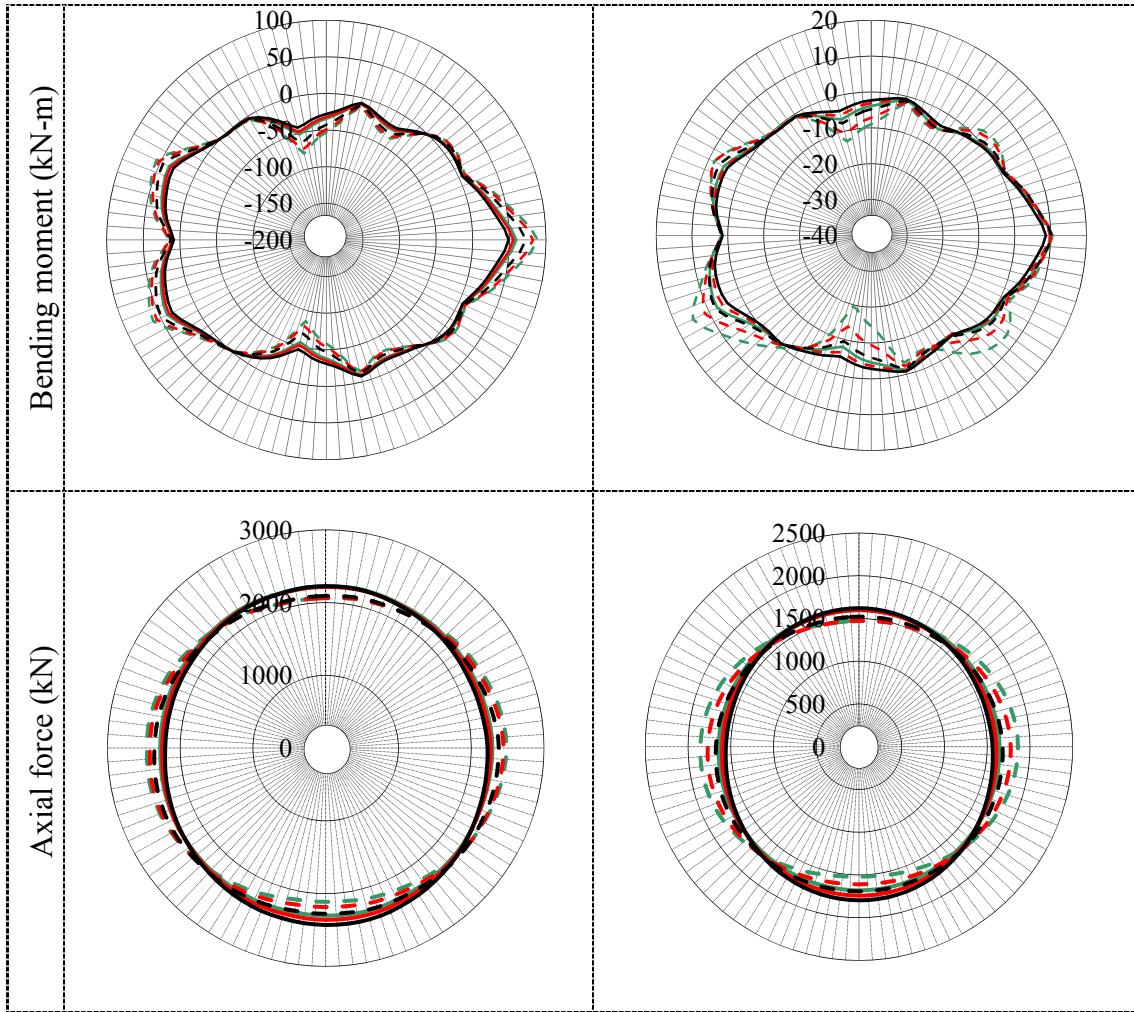
	$k_t/k_n = 0$	$k_t/k_n = 1/3$	$k_t/k_n = 1$
Type 0 (no τ_0)	Case10	Case20	Case30
Type 1 (with τ_0)	Case11	Case21	Case31
Segment			

Appendix B. Data for building *M*, *N*, *e/t* graphs.

Table B.1. Maximum and minimum bending moment (deep tunnel).

a) Maximum bending moment M^+ (kN-m/m).

Load model	Case	$k = 10$MN/m³			$k = 50$MN/m³			$k = 100$MN/m³			$k = 500$MN/m³			$k = 1000$MN/m³		
		M^+	(a)	(b)	M^+	(a)	(b)	M^+	(a)	(b)	M^+	(a)	(b)	M^+	(a)	(b)
	10	228.0			59.3			31.0			10.6			9.9		
Type 0	20	216.2	-5.2%		55.4	-6.6%		28.9	-6.8%		10.0	-5.3%		8.3	-16.7%	
	30	195.9	-14.1%		49.0	-17.3%		25.7	-17.2%		8.7	-17.5%		5.9	-40.9%	
	11	343.6		50.7%	88.6		49.4%	45.3		46.2%	15.0		42.1%	22.6		127.5%
Type 1	21	325.2	-5.4%	50.4%	82.4	-7.0%	48.8%	42.1	-7.2%	45.5%	11.3	-24.9%	12.7%	8.9	-60.8%	7.0%
	31	294.0	-14.4%	50.1%	72.5	-18.1%	47.9%	37.0	-18.4%	44.2%	10.3	-31.3%	18.3%	9.4	-58.3%	60.6%

Note: column (a) shows the influence of tangential spring stiffness, and (b) shows the influence of the load model

b) Minimum bending moment M^- (kN-m/m).

Load model	Case	$k = 10$MN/m³			$k = 50$MN/m³			$k = 100$MN/m³			$k = 500$MN/m³			$k = 1000$MN/m³		
		M^-	(a)	(b)	M^-	(a)	(b)	M^-	(a)	(b)	M^-	(a)	(b)	M^-	(a)	(b)
	10	-205.0			-55.8			-30.6			-7.9			-6.1		
Type 0	20	-194.4	-5.2%		-51.6	-7.5%		-28.3	-7.3%		-6.4	-19.9%		-4.0	-34.5%	
	30	-176.1	-14.1%		-45.7	-18.1%		-24.8	-18.7%		-5.1	-35.5%		-2.8	-53.7%	
	11	-309.4		50.9%	-85.4		53.1%	-48.0		57.1%	-19.6		146.4%	-34.7		467.0%
Type 1	21	-292.2	-5.6%	50.3%	-78.7	-7.9%	52.4%	-43.4	-9.5%	53.3%	-13.8	-29.6%	116.5%	-11.9	-65.6%	197.8%
	31	-264.4	-14.5%	50.2%	-68.6	-19.7%	50.2%	-37.0	-22.8%	49.1%	-9.5	-51.4%	85.8%	-5.3	-84.7%	87.9%

Note: column (a) shows the influence of tangential spring stiffness, and (b) shows the influence of the load model

Table B.2. Maximum and minimum bending moment (shallow tunnel).

a) Maximum bending moment M^+ (kN-m/m).

Load model	Case	$k = 10$MN/m³			$k = 50$MN/m³			$k = 100$MN/m³			$k = 500$MN/m³			$k = 1000$MN/m³		
		M^+	(a)	(b)	M^+	(a)	(b)	M^+	(a)	(b)	M^+	(a)	(b)	M^+	(a)	(b)
	10	89.7			23.3			12.1			3.0			2.1		
Type 0	20	85.9	-4.2%		22.0	-5.5%		11.4	-5.4%		2.9	-4.2%		2.1	0.6%	
	30	79.3	-11.6%		19.9	-14.7%		10.3	-14.7%		2.7	-11.5%		1.9	-9.4%	
	11	137.7		53.6%	35.3		51.7%	18.0		48.7%	4.9		63.0%	4.2		97.0%
Type 1	21	131.3	-4.7%	52.8%	33.2	-6.1%	50.7%	16.9	-6.1%	47.6%	3.9	-20.6%	35.1%	2.8	-32.8%	31.7%
	31	120.1	-12.8%	51.6%	29.7	-16.0%	49.4%	15.1	-16.1%	46.3%	3.1	-37.0%	16.1%	2.0	-52.6%	3.0%

Note: column (a) shows the influence of tangential spring stiffness, and (b) shows the influence of the load model

b) Minimum bending moment M^- (kN-m/m).

Load model	Case	$k = 10$MN/m³			$k = 50$MN/m³			$k = 100$MN/m³			$k = 500$MN/m³			$k = 1000$MN/m³		
		M^-	(a)	(b)	M^-	(a)	(b)	M^-	(a)	(b)	M^-	(a)	(b)	M^-	(a)	(b)
	10	-82.9			-23.1			-12.8			-3.4			-2.1		
Type 0	20	-79.0	-4.7%		-21.6	-6.2%		-11.8	-7.8%		-2.9	-12.7%		-1.6	-20.4%	
	30	-73.1	-11.8%		-19.3	-16.4%		-10.6	-17.1%		-2.6	-21.9%		-1.4	-30.9%	
	11	-127.4		53.6%	-36.2		57.1%	-20.3		58.5%	-6.6		97.2%	-6.8		230.4%
Type 1	21	-120.9	-5.1%	52.9%	-33.1	-8.7%	52.9%	-18.2	-10.0%	54.7%	-5.2	-21.7%	76.9%	-3.6	-46.6%	121.5%
	31	-110.1	-13.6%	50.5%	-29.1	-19.8%	50.8%	-15.7	-22.5%	48.2%	-4.1	-38.4%	55.4%	-2.5	-63.8%	73.1%

Note: column (a) shows the influence of tangential spring stiffness, and (b) shows the influence of the load model

Table B.3. Maximum axial force N_{max} (kN/m) (deep tunnel).

Load model	Case	$k = 10$MN/m³			$k = 50$MN/m³			$k = 100$MN/m³			$k = 500$MN/m³			$k = 1000$MN/m³		
		N_{max}	(a)	(b)	N_{max}	(a)	(b)	N_{max}	(a)	(b)	N_{max}	(a)	(b)	N_{max}	(a)	(b)
	10	2448			2312			2194			1681			1482		
Type 0	20	2468	0.8%		2364	2.2%		2246	2.4%		1742	3.6%		1547	4.4%	
	30	2532	3.4%		2432	5.2%		2314	5.5%		1797	6.9%		1580	6.6%	
	11	2664		8.8%	2486		7.5%	2358		7.5%	1860		10.6%	1716		15.8%
Type 1	21	2630	-1.3%	6.6%	2444	-1.7%	3.4%	2314	-1.9%	3.0%	1780	-4.3%	2.2%	1545	-10.0%	-0.1%
	31	2574	-3.4%	1.7%	2390	-3.9%	-1.7%	2258	-4.2%	-2.4%	1708	-8.2%	-5.0%	1517	-11.6%	-4.0%

Note: column (a) shows the influence of tangential spring stiffness, and (b) shows the influence of the load model

Table B.4. Maximum axial force N_{max} (kN/m) (shallow tunnel).

Load model	Case	$k = 10MN/m^3$			$k = 50MN/m^3$			$k = 100MN/m^3$			$k = 500MN/m^3$			$k = 1000MN/m^3$		
		N_{max}	(a)	(b)	N_{max}	(a)	(b)	N_{max}	(a)	(b)	N_{max}	(a)	(b)	N_{max}	(a)	(b)
Type 0	10	655			629			599			450			369		
	20	693	5.8%		667	6.0%		637	6.2%		483	7.3%		401	8.7%	
	30	739	12.7%		713	13.3%		680	13.6%		514	14.2%		425	15.1%	
Type 1	11	732		11.7%	678		7.7%	644		7.5%	499		10.9%	428		15.9%
	21	722	-1.4%	4.1%	671	-1.0%	0.5%	637	-1.1%	0.0%	480	-3.8%	-0.6%	393	-8.1%	-2.0%
	31	719	-1.8%	-2.6%	668	-1.4%	-6.4%	632	-1.9%	-7.2%	468	-6.2%	-8.9%	384	-10.2%	-9.6%

Note: column (a) shows the influence of tangential spring stiffness, and (b) shows the influence of the load model

Table B.5. Maximum absolute moment M_{max} (kN-m/m), associated axial force N_{assoc} (kN/m), and normalized eccentricity e/t (deep tunnel).

Load model	Case	$k = 10\ MN/m^3$				$k = 50\ MN/m^3$				$k = 100\ MN/m^3$				$k = 500\ MN/m^3$				$k = 1000\ MN/m^3$			
		θ	M_{max}	N_{assoc}	e/t	θ	M_{max}	N_{assoc}	e/t	θ	M_{max}	N_{assoc}	e/t	θ	M_{max}	N_{assoc}	e/t	θ	M_{max}	N_{assoc}	e/t
Type 0	10	90	228.0	2448	0.252	90	59.3	2290	0.070	90	31.0	2164	0.039	90	10.6	1645	0.017	90	9.9	1445	0.019
	20	90	216.2	2428	0.241	90	55.4	2266	0.066	90	28.9	2138	0.037	90	10.0	1607	0.017	90	8.3	1396	0.016
	30	90	195.9	2390	0.221	90	49.0	2224	0.060	90	25.7	2096	0.033	90	8.7	1563	0.015	90	5.9	1373	0.012
Type 1	11	90	343.6	2664	0.349	90	88.6	2486	0.096	194.4	48.0	2028	0.064	194.4	19.6	1548	0.034	190.8	34.7	1390	0.067
	21	90	325.2	2630	0.334	90	82.4	2444	0.091	194.4	43.4	2094	0.056	194.4	13.8	1624	0.023	194.4	11.9	1468	0.022
	31	90	294.0	2574	0.309	90	72.5	2380	0.082	90	37.0	2246	0.045	90	10.3	1681	0.017	90	9.4	1433	0.018

Table B.6. Maximum absolute moment M_{max} (kN-m/m), associated axial force N_{assoc} (kN/m), and normalized eccentricity e/t (shallow tunnel).

Load model	Case	$k = 10\ MN/m^3$				$k = 50\ MN/m^3$				$k = 100\ MN/m^3$				$k = 500\ MN/m^3$				$k = 1000\ MN/m^3$			
		θ	M_{max}	N_{assoc}	e/t	θ	M_{max}	N_{assoc}	e/t	θ	M_{max}	N_{assoc}	e/t	θ	M_{max}	N_{assoc}	e/t	θ	M_{max}	N_{assoc}	e/t
Type 0	10	90	89.7	643	0.377	90	23.3	597	0.105	194.4	12.8	596	0.058	194.4	3.4	449	0.020	244.8	2.1	353	0.016
	20	90	85.9	637	0.364	90	22.0	589	0.101	194.4	11.8	631	0.050	194.4	2.9	479	0.017	90	2.1	312	0.019
	30	90	79.3	626	0.342	194.4	19.9	704	0.076	194.4	10.6	672	0.043	90	2.7	382	0.019	90	1.9	296	0.018
Type 1	11	90	137.7	732	0.508	194.4	36.2	548	0.179	194.4	20.3	524	0.105	194.4	6.6	384	0.047	190.8	6.8	308	0.059
	21	90	131.3	722	0.492	90	33.2	663	0.135	194.4	18.2	566	0.087	194.4	5.2	425	0.033	194.4	3.6	352	0.028
	31	90	120.1	702	0.462	90	29.7	640	0.125	194.4	15.7	615	0.069	194.4	4.1	462	0.024	194.4	2.5	384	0.017